Plastic Dynamic Response of Simply Supported Thick Square Plates Subject to Localised Blast Loading

N. Mehreganian[a], A. S. Fallah[b,c*], L.A. Louca[a]

[a] *Department of Civil & Environmental Engineering, Skempton Building, South Kensington Campus, Imperial College London, London SW7 2AZ, UK*

[b] *Department of Aeronautics, Roderic Hill Building, South Kensington Campus, Imperial College London, London SW7 2AZ, UK*

[c] *Department of Mechanical, Aerospace and Civil Engineering, Brunel University London, Uxbridge UB8 3PH, UK*

ABSTRACT

Localised blast loads due to proximal charges are encountered in a variety of circumstances. This paper proposes an analytical solution for the dynamic plastic response of a rigid-perfectly plastic thick square plate subject to a localised explosion. The proposed model is an extension of the analytical model proposed by Micallef et al [1] to study circular plates which is adopted and modified in order to study impulsively loaded square plates where the effect of shear deformation is included. A piecewise continuous blast load function was assumed with axisymmetric spatial distribution of constant pressure in the central zone and exponentially decaying beyond it. Using the constitutive framework of limit analysis and incorporating the interactions between bending moment and transverse shear forces in the analyses, transverse displacement and response duration were examined on three classes of plates, classified according to the length to thickness ratio parameter ν. The results were furnished in terms of the impulsive velocity, which is a function of the localised blast load parameters. A theoretical solution for plates with $\nu > 2$ was sought for the non-impulsive blast loads. Parametric studies were performed to elucidate the effect of loading parameters and plate thickness on the permanent deformation. The theoretical solutions have been found generic and can predict, by the correct choice of the load parameters, the dynamic response of most blast load scenarios brought about by proximal or distal charges. It was found that, for proximal impulsive blasts, the effect of transverse shear becomes irrelevant for even moderate values of ν, which effect is inconsequential on both central and endpoint displacements at discontinuous interface in the range of $\nu > 5$. Since the short duration pulse is of concern, localised pressure loads affect only a small area of the plated structures. Thus, whilst the

---

[*] To whom correspondence should be addressed:

Email: as3@imperial.ac.uk (Arash S. Fallah)

Tel.: +44 (0) 2075945140

Fax: +44 (0) 2075941974

1 *theoretical treatments also examine the clamped plates, the boundary conditions in such loads do not*

2 *influence the overall response of the structure compared to the static or global blast loads.*

3 *Keywords: Transverse shear, slenderness ratio, localised blast, displacement at discontinuous*

4 *interface, travelling plastic hinge*

5

Nomenclature

Latin upper and lower case

$A - G$	Integration constants; [various]
M_0	Maximum plastic bending moment; $[MLT^{-2}]$
Q_0	Maximum transverse shear force; $[MT^{-2}]$
W_i	Maximum transverse displacement at the ith phase; [L]
$\dot{W}_i$	Transverse velocity at the ith phase; $[LT^{-1}]$
$\ddot{W}_i$	Transverse acceleration at the ith phase; $[LT^{-2}]$
T_f	Final time of motion; [T]
$\bar{T}_f$	Dimensionless final time of motion
V_1	Impulsive velocity of localised load; $[LT^{-1}]$
a	Loading parameter; [1]
b	Loading exponent; $[m^{-1}]$
$\bar{m}_i$	Dimensionless moment normal to i ; [1]
p_0	Maximum overpressure; $[ML^{-1}T^{-2}]$
p_c	Static collapse pressure; $[ML^{-1}T^{-2}]$
$p_1(x,y)$	Spatial part of pressure pulse load; $[ML^{-1}T^{-2}]$
$p_2(t)$	Temporal part of pressure pulse load; [1]
r_e	Radius of central uniformly-loaded region; [L]
$\bar{w}_f$	Dimensionless maximum final transverse displacement; [1]

$\bar{\bar{w}}$	$M_0/(L^2\mu)$ [1]	
Greek upper and lower case		
α	Impulsive velocity parameter; $[L^2]$	
β	Static collapse pressure co-efficient; $[L^3]$	
ξ	Plastic hinge generalised coordinate; [1]	
$\dot{\theta}_i$	Rotational velocity in the direction i; $[T^{-1}]$	
η	Dynamic load factor; [1]	
η_{crit}	Critical dynamic load factor; [1]	
$\bar{\lambda}$	Dimensionless kinetic energy [1]	
μ	Areal density; $[ML^{-2}]$	
ρ	Material density; $[ML^{-2}]$	
τ^*	$\mu V_1 L^2/M_0$ [T]	
τ	Duration of the pulse; [T]	
σ_0	Static yield stress; $[MLT^{-2}]$	
ν	Slenderness ratio [1]	
γ	Transverse shear strain [1]	
τ^*	$\mu L^2 V_1/M_0$ [1]	
ψ'	Energy effectiveness [1]	

6

1   Introduction

8   Blast load overpressures induced by explosion of proximal or distal charges can have detrimental

9 effects and cause injury, loss of life or damage to property, infrastructure, equipment, and vehicles. As

10 the blast overpressure diminishes exponentially with distance from its source, close-in blasts are of more

11 importance and can potentially ensue more severe localised damage. Consequently, mitigating the

12 effects of close-in threats is of prime significance in civil, aeronautical, offshore, and mechanical

13 engineering.

14   In fact, many authors have assessed the effects of blast phenomenon on structural systems [2]–[6],

15 which led to classification of three failure modes for beam systems by Menkes and Opat [7] as Mode I:

16 large inelastic deformation, Mode II: tensile tearing in outer fibres and Mode III: transverse shear failure

17 at the support(s) for uniformly blast loaded beams. This classification incorporated the plated structures

18 with various boundary conditions in [8] and was further extended to the case of localised blasts [9].

19 Current investigations on the performance of plated elements, however, have primarily focused on the

distant blast waves giving rise to uniform or nearly-uniform pressure distribution and globalised response, while the localised blast response of rectangular plates has not been assessed in detail.

Most structural systems are made of individual quadrangular plated elements which are made of ductile metallic materials with significant post yield deformation capacity. These materials are often idealised with rigid-perfectly plastic behaviour in an analytical treatment. In most cases the rigid-perfectly plastic idealisation with consideration of the membrane and bending forces suffices to predict the dynamic performance of the structural systems with reasonable accuracy. There are, however, cases where the influence of the transverse shear cannot be ignored. The plated elements in these cases are often sufficiently thick, such that the transverse shear effects play an important role on the overall dynamic plastic behaviour of the structure [1].

The transverse shear response is an important concept during the early stage response of the structural elements [10]–[12]. The influence of transverse shear on uniformly impulsively loaded beams and circular plates has been examined by Jones and co-authors [13]–[18] who have classified the thick circular plates and shells according to the ratio of static plastic shear capacity to plastic bending moment ($\nu = Q_0R/2M_0$), with R being the radius of the plate. With increased thickness of plate, the plastic work rate due to bending transcends that of the membrane [19]. Further increase in thickness renders the effects of rotatory inertia and shear significant (Fig. 1-Fig. 2) although the effect of the former is not nearly as important as the effect of the latter. Rotatory inertia effects would contribute toward the moment for moderately-stocky circular plates ($L/H > 3/2$) or beams subjected to uniform blasts [13], [14]. However, the theoretical study sought in the case of class II (moderate stocky) circular plates- where ν is in the range of $\nu = 1.5 < Q_0R/2M_0 < 2$- showed that combined effect of the rotatory inertia and transverse shear effect would only improve the accuracy of maximum permanent displacements by only 11%-14% compared to those due to transverse shear effect alone [13]. Li [10] investigated the continuity conditions of shearing interface and bending interface of stationery and moving hinge and discussed that the localised shear response becomes the dominant mode when the transverse shear conditions are satisfied. Li and Huang [20] showed that while the inner plastic region undergoes a small transverse shear force, the transverse shear deformation increases rapidly in the outer plastic region. On the other hand, the bending moment is large throughout the plate and decreases only rapidly near the supports. It follows that the transverse shear forces induce shear sliding at the support at the interface of which the deformation profile is discontinuous.

This paper is an extension of the earlier work on uniformly distributed pulse pressure effects on circular plates to investigate the transverse shear sliding in square plates induced by localised blasts. Although the mathematical procedure incorporates the classical plate theories of plasticity such as those found in [21], [22], the physics of the localised blast entails intrinsically different phenomenon than uniform pressure loads commonly practised in the literature. Hence, the theoretical treatment is carried out by incorporating the modified spatial blast- reflective of most precise idealisation of localised blast

loads. While the major thrust behind this work is the focus on impulsively loaded plates, an analysis of the dynamic loads is also presented for plates of moderate thickness ($L/H > 4$) that are not considered as thin plates nor membranes. Thus, the outline of this work in six sections is as follows: following this introduction, the characteristic of the load and the equations of motion are presented in section 2. Section 3 discusses the static transverse shear loads and the associated collapse pressure, while this is extended to the dynamic collapse pressure of section 4, considering various ranges of ν for simply supported and clamped plates, followed by numerical analyses of section 5. Finally, the conclusions of this study are presented in section 6.

It is recognised that the study of simply supported plates along with fully clamped plates will furthermore provide lower and upper bounds on the deformation which are helpful in analysis of real situations where semi-rigid connections are used and have not been completely/properly quantified. It is also appreciated that the explicit theoretical solutions for rectangular plates may not be straightforwardly determined, as the potential energy functional (i.e. $\int p_0 \dot{w}(x, y, t) e^{-b\sqrt{x^2+y^2}}$) over such manifolds leads to an error function.
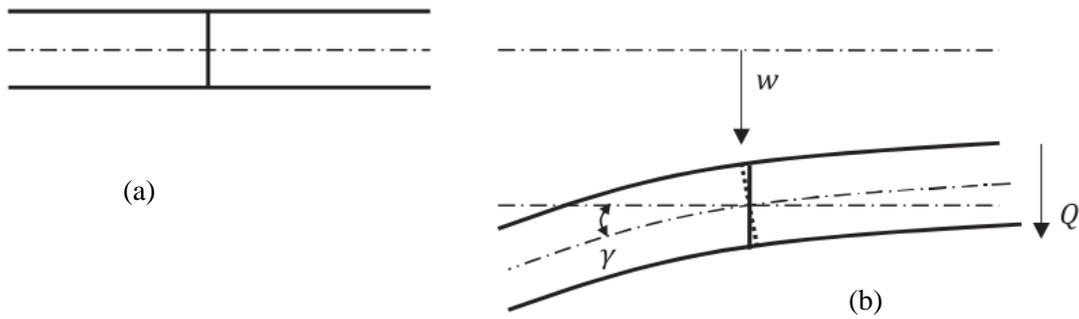
Fig. 1-Pure plate shearing (a) undeformed shape (b) deformed shape
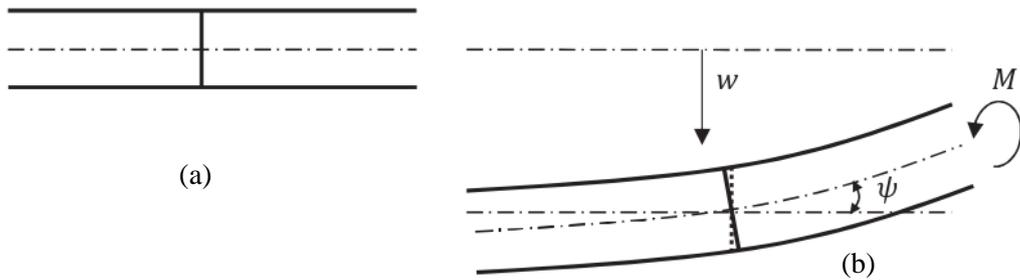
Fig. 2- Pure plate bending (a) undeformed shape (b) deformed shape (after [21])

2 Problem definition

2.1 Structure and loading

The structural model studied here is an idealised initially flat, monolithic, ductile metallic square plate with side length $2L$, thickness of H and areal density of $\mu = \rho H$, pinned along its edges and subjected to lateral blast load. The loading characterises a generic blast load, which is multiplicatively decomposable to spatial (load shape) and temporal (pulse shape) parts, i.e. $P(x, y, t) = p_1(x, y)p_2(t)$.

The spatial variation of the load, as shown by [23] and Fig. 3, maintains a uniform pressure within the central disk of radius r_e before decaying exponentially along radial coordinate r, as given by Eqn. (1) (Part II). Thus, the load is axisymmetric and reduces the domain of study to only one quarter of the plate (considering the plate has only 2 axes of symmetry). The temporal pulse shape of the blast varies as a function of the type of detonation. While the pulse shape can have a significant influence on the plastic dynamic response of the non-impulsively loaded structure, its effect can be eliminated by utilising Youngdahl's correlation parameters [24]–[27], the efficacy of which is confirmed for monotonically decaying pulses by [28]. For impulsive blasts, the pulse shape has no intrinsic effect on the system. For the study of non-impulsive blasts, a rectangular pulse shape is assumed here, given by Eqn. (2).

$$p_1(r) = \begin{cases} p_0 & 0 \leq r \leq r_e \\ p_0 a e^{-br} & r_e \leq r \leq R \end{cases} \tag{1}$$

$$p_2(t) = \begin{cases} 1 & for\ 0 \leq t \leq \tau \\ 0 & for\ t \geq \tau \end{cases} \tag{2}$$

In Eqn. (1), $r = \sqrt{x^2 + y^2}$, and $a = e^{br_e}$ is the loading parameter. The loading parameters and exponents a and b, respectively, can be obtained through curve fitting to the pressure data from commercial Finite Element hydrocodes or tests, considering the explosive type, geometry and stand-off from the target. Thus, the form of Eqn. (2) would be universal and with a correct choice of b, r_e can represent various loading scenarios from localised blast to global blast loads. A curve fit of load shape to the experimental results of Tyas et al. [29] is presented in Fig. 4.

By the correct choice of load parameters, the assumed blast function delineates a wide spectrum of practical blast scenarios brought about by either proximal or distal charges.
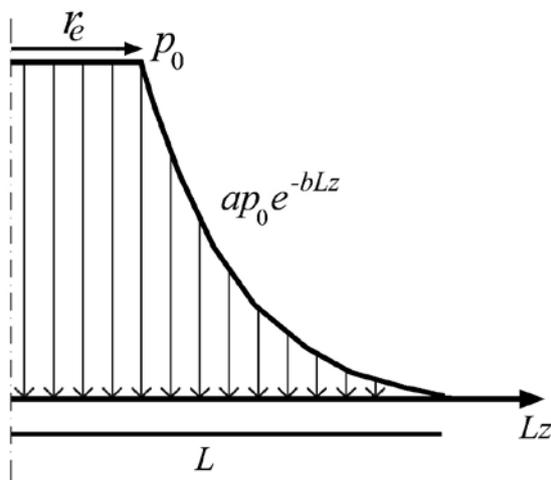
Fig. 3- Spatially exponential distribution of load
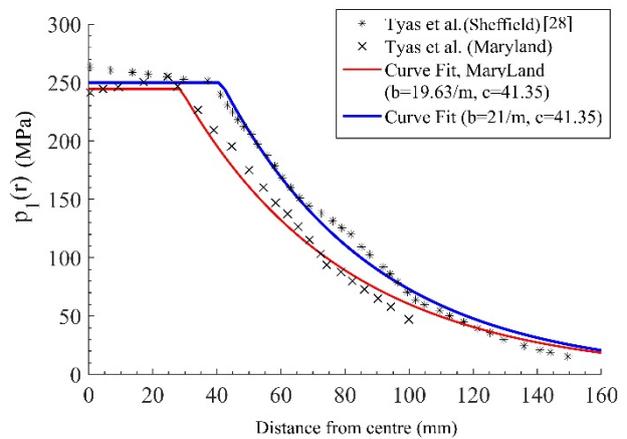
Fig. 4- Validations of blast spatial function to the experimental results of [29]

2.2 Equations of motion

The governing equations of motion (or dynamic equilibrium) in Cartesian coordinates for the dynamic performance of a plate loaded laterally are given as:

$$\frac{\partial Q_x}{\partial x} + \frac{\partial Q_y}{\partial y} = \mu \ddot{w} - P(x, y, t) \tag{3}$$

$$\frac{\partial M_x}{\partial x} + \frac{\partial M_{xy}}{\partial y} - Q_x = I_r \partial^2 \psi / \partial t^2 \tag{4}$$

$$\frac{\partial M_y}{\partial y} + \frac{\partial M_{xy}}{\partial x} - Q_y = I_r \partial^2 \psi / \partial t^2 \tag{5}$$

In Eqns. (3)-(5), I_r is the rotatory inertia, the rotation of a line- in x direction is defined by $\frac{\partial w}{\partial x} = \psi + \gamma$ – which is the same as the rotation of a fibre originally normal to the initial mid-surface due to bending, and $\gamma = \partial w / \partial x - \psi$ is the transverse shear strain. Thus, $\dot{k}_x = \partial \dot{\psi} / \partial x$, $\dot{k}_y = \partial \dot{\psi} / \partial x$, and $\dot{k}_{xy} = -\partial^2 \dot{w} / \partial y \partial x$ describe the curvature rates due to bending in x, y, and twisting in xy directions, respectively. When the transverse shear strains are not negligible compared to the deformation gradients (rotations), the transverse shear and rotatory inertia contribute to the bending dynamic equilibrium equations of Eqns. (4)-(5). The right-hand side of these equations vanish in the absence of rotatory inertia effects, the scenario assumed here.

By referring to the dynamic continuity conditions across discontinuity front in beams and circular plates, it is noted that for quadrangular plates, $[M_i] = -\dot{Z} I_r [\dot{\psi}_i]$, $[Q_i] = -\mu \dot{Z} I_r [\dot{w}]$, where, for example, the notation $[\dot{\psi}_i] = \dot{\psi}_2 - \dot{\psi}_1$ refers to the difference of the quantity $\dot{\psi}$ across the discontinuity interface, i.e. the jump, as in [16], [17]. The boundary conditions of simply supported plate are given by:

$$M_n|_{z=1} = 0, \quad Q_x|_{x=L, y=0} = Q_y|_{y=L, x=0} = -Q_0, \quad w|_{z=1} = 0, \quad \dot{w}|_{z=0} = \dot{W} \tag{6a-d}$$

It is pragmatic to introduce an auxiliary dimensionless coordinate z as illustrated in Fig 5 (b), for the plate whose plastic hinge lines lie on the diagonals of the square and construct the collapse mechanism. It is rather a straightforward task to show that the theoretical solutions emerging from the dynamic equilibrium analysis along the plastic hinge lines in Fig 5 (a)- characterised with $r = zL = \sqrt{x^2 + y^2}$ -conform to the theoretical solutions characterised with the generalised auxiliary coordinate z as in Fig 5 (b). Thus, in a similar procedure to the work of Cox and Morland [30], the bending moments across the structure interface may be expressed in terms of a moment function $f(z)$:

$$M_x = M_0 + x^2 f(z) \tag{7}$$

$$M_y = M_0 + y^2 f(z) \tag{8}$$

$$M_{xy} = xyf(z) \tag{9}$$

1   The above expressions satisfy the moment boundary conditions at the plate centre and at the
2   supports, they nevertheless should meet the dynamic continuity conditions and the conservation of
3   linear and angular momenta, i.e. they should satisfy the admissibility condition and nowhere violate the
4   yield condition. Substituting the Eqns. (7)-(9) in the expression of principle moments given by [21],
5   [31], it turns out that the principle moments across the plate would be bound to

$$\mathrm{M}_1 = (M_x + M_y)\,/2 - \frac{1}{2}\left[(M_x - M_y)^2 + 4M_{xy}^2\right]^{\frac{1}{2}} = M_0 \tag{10}$$

$$-M_0 \le \mathrm{M}_2 = (M_x + M_y)\,/2 + \frac{1}{2}\left[(M_x - M_y)^2 + 4M_{xy}^2\right]^{\frac{1}{2}} \le M_0 \tag{11}$$

6   where M_n is the bending moment normal to the generalised coordinate in direction n, given in [31].
7   Provided the rotatory inertia effects are ignored, combining Eqns. (7)-(9) with (3)-(5) yields:

$$6f + 6z\frac{\partial f}{\partial z} + z^2\frac{\partial^2 f}{\partial z^2} = \mu\ddot{w} - p_0\,, \qquad\qquad 0 \le z \le r_e/L \tag{12}$$

$$6f + 6z\frac{\partial f}{\partial z} + z^2\frac{\partial^2 f}{\partial z^2} = \mu\ddot{w} - ap_0 e^{-bLz} \qquad\qquad r_e/L \le z \le 1 \tag{13}$$

8   This linear non-homogenous, second-order, Ordinary Differential Equation (ODE) with constant
9   coefficients is solved for various loading conditions that give rise to the corresponding velocity profile
10   which must satisfy the yield condition. It should be noted that the principle moment M_2 and transverse
11   shears may be written as Eqns. (14)-(16).

(a)   (b)
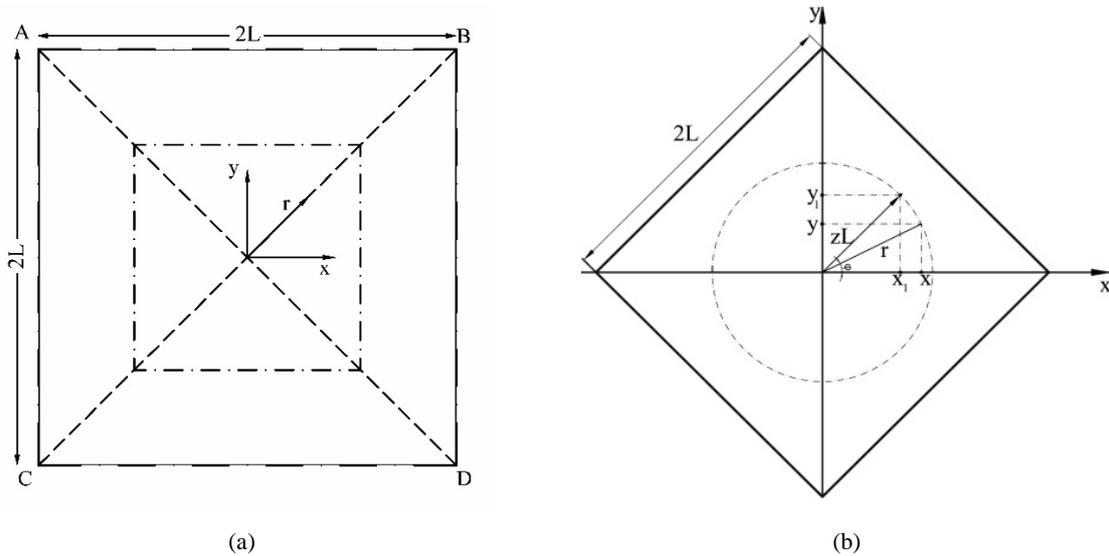
Fig 5- (a) Top view of a simply-supported square plate (coordinates x, y, r and dimensionless parameter z are shown), (b) the plate with side lengths 2L whose diagonals are in the Cartesian Coordinate axes

12

$$\frac{M_2}{M_0} = 1 + z^2 L^2 f(z)/M_0 \tag{14}$$

$$Q_x = x\left(3f + \frac{z\partial f}{\partial z}\right) \tag{15}$$

$$Q_y = y\left(3f + \frac{z\partial f}{\partial z}\right) \tag{16}$$

2.3 Yield Surface

By referring to the influence of transverse shear on beams and circular plates, it turns out that the transverse shear forces at the edges should be large at the start of motion to induce shear sliding. Considering Drucker's plasticity postulates (stability conditions) and ignoring the rate sensitivity effects, it is assumed that the plastic flow is controlled by interaction of transverse shear and bending moment, characterised by the extended yield surface square and its associated flow rule. The square yield surface circumscribes the Tresca's yield surface, as shown in Fig. 6, and the direction of strain rates remains orthogonal to the yield surface at any point.

$$M_0 = \sigma_0 H^2/4 \tag{17}$$

$$Q_0 \cong \frac{\sigma_0 H}{2} \tag{18}$$

In Eqn.'s (17) and (18) M_0 and Q_0 are the maximum plastic bending moment per unit length and the maximum lateral shear force per unit length, respectively. It turns out that the plastic flow is defined by the side AC of the original square yield surface (and along the plane extruded by side AC in the extended yield surface).

It is beneficial to define the following dimensionless parameters:

$$\overline{q_d} = Q_d/Q_0, \quad \overline{m} = M_2/M_0, \quad \bar{\lambda} = \frac{V_1^2 L^2 \mu}{M_0 H}, \quad \overline{w}_f = W_f/H,$$

$$\tau^* = \mu L^2 V_1/M_0, \quad \overline{\overline{w}} = \frac{M_0}{L^2 \mu} \quad \nu = Q_0 L/2M_0 \tag{19a-g}$$

The dimensionless parameter ν in Eqn. (19-g) characterises the ratio of plastic shear to bending mechanism and reduces to the slenderness ratio L/H for the prismatic sections, which is a measure of plate aspect ratio and is purely a parameter of geometrical dimensions. It should be stressed that the transverse shear hinges do not develop when the material hardening is ignored [11].

8
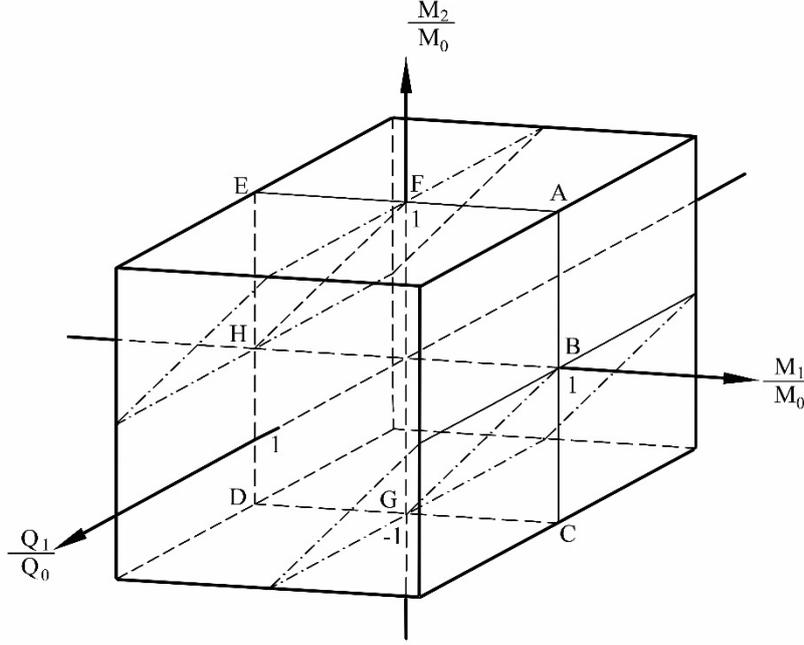
Fig. 6 Interaction yield curve of $(-.-)$ **Tresca vs** $(-)$ **Square yield surface**

2.4 Impulsive loading

An impulsive blast load is characterised by very short pulse duration $(\tau \rightarrow 0)$ and very high amplitude $(\eta \rightarrow \infty$ or $p_0 \gg p_c)$. The impulse load, as defined by Dirac delta function, may be replaced with equivalent impulsive velocity. In such a case, the total impulse transmitted to the system is equated to the change in linear momentum of the system, hence, the conservation of momentum at the onset of motion $(t = 0)$implies:

$$\int_0^{\frac{r_e}{L}} L^2 \tau p_0 z dz + \int_{\frac{r_e}{L}}^1 L^2 \tau p_0 a e^{-bLz} z dz = \int_0^1 L^2 \mu V_1 z dz \tag{20}$$

The solution to the Eqn. (20) yields:

$$V_1 = \frac{\tau p_0}{\mu}\left(\frac{\alpha}{L^2}\right) \tag{21}$$

$$\alpha = \left[\frac{r_e^2 b^2 - 2ae^{-Lb}(bL + 1) + 2r_e b + 2}{b^2}\right] \tag{22}$$

In most typical cases of localised blasts, the ratio of stand-off to charge diameter varies between 0.5 and 5, corresponding to the normalised loading radius $r_e/L \leq 0.2$, assuming small values, and the loading exponent varying as $40 \leq b \leq 100$. Thus, the impulse parameter α would have a range of $\alpha \leq 0.2L^2$, as observed in the Fig. 7. It transpires that for the typical impulsive localised blasts, the impulsive

1   velocity is independent of the loading distribution and is directly proportional to the peak pressure load

2   and duration of the pulse pressure.

3
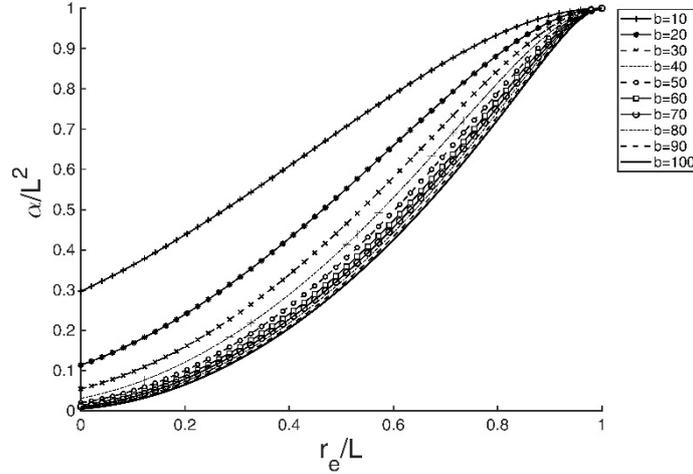
Fig. 7- Variation of α with the radius of the blast load

4

3   Static Collapse Pressure

6   The lower bound of the static plastic collapse is determined by solution to the equilibrium equations,

7   which were cast in the form of Eqns. (12), and (13) and are given as follows:

$$f(z) = \begin{cases} -\dfrac{p_c}{6} + \dfrac{A_1}{z^2} + \dfrac{B_1}{z^3} & 0 \leq z \leq r_e/L & \textbf{(23a)} \\[3mm] \dfrac{-ap_c e^{-bLz}(bLz + 2)}{(bLz)^3} + \dfrac{C_1}{z^2} + \dfrac{C_2}{z^3} & r_e/L \leq z \leq 1 & \textbf{(23b)} \end{cases}$$

8   The arbitrary constants A_1, B_1, C_1 and C_2 are obtained in Eqns. (24a-c) owing to the continuity of

9   moment function $f(z)$ and its derivative at $z = r_e/L$.

10

$$\begin{cases} A_1 = B_1 = 0 & \textbf{(24a)} \\[3mm] C1 = \dfrac{-p_c((br_e)^2 + 2br_e + 2)}{2(Lb)^2} & \textbf{(24b)} \\[3mm] C2 = \dfrac{p_c((br_e)^3 + 3(br_e)^2 + 6br_e + 6)}{3(Lb)^3} & \textbf{(24c)} \end{cases}$$

11

12   The condition of $M_2 = 0$ along the plate periphery in Eqn. (14) yields the lower bound to the plastic

13   collapse as

10

$$p_c = \frac{M_0}{\beta L^2} \tag{25}$$

where the static collapse coefficient β is given by:

$$\beta = \left(\frac{3Lr_e{}^2 - 2r_e{}^3}{6L^3}\right) + \frac{(ae^{-Lb}(Lb+2) + b^2 r_e(L - r_e) + bL - 2br_e - 2)}{L^3 b^3} \tag{26}$$

In a similar fashion, by considering a conical velocity as $\dot{w} = \dot{W}(1 - z)$, the upper bound collapse load is determined as $p_u = M_0/\beta_2 L^2$ from the energy equilibrium Eqn. (27), where $\beta_2 = \beta$. Thus, it can be shown that the upper bound and lower bound static collapse loads are identical, the plastic collapse load so obtained is, therefore, exact.

$$\iint M_x \dot{k}_x + M_y \dot{k}_y + 2M_{xy} \dot{k}_{xy} dx dy - \int (p(x,y,t) - \mu\ddot{w})\dot{w} dA = 0 \tag{27}$$

The transverse shear at the boundary is determined by Eqn. (28), by evaluating Eqn. (15) and using constants determined by Eqn.'s (24 a-c) and condition of Eqn. (6-b). An identical expression would be obtained if Eqn. (16) was employed.

$$\left|\frac{Q_s}{Q_0}\right| = -\frac{\left[(Lb+1)e^{-Lb+br_e} - \frac{1}{2}b^2 r_e^2 - br_e - 1\right]}{2L^2 b^2 \beta \nu} \tag{28}$$

4   Dynamic Collapse Pressure

Through consideration of static admissibility, and defining the dynamic load factor as $\eta = p_0/p_c$, it can be shown that a critical value for η exists which prevents yield violation in the case of infinitesimal deformations and gives rise to stationery plastic hinge [26]. For square plates subjected to uniform blasts, $\beta = 1/6$ thus, $\eta = 2$ while for the localised blast, the range of dynamic load factor may be expressed by:

$$\eta \leq \left|\frac{12\beta}{12\beta - 1}\right| = \eta_{crit} \tag{29}$$

Eqn. (29) is obtained through a similar procedure as [26]. In a similar fashion to the static case, by considering the shear sliding at the supports (i.e. Eqn. (6-b), the dynamic transverse shear is determined as:

$$\left|\frac{Q_d}{Q_0}\right| = \left(\frac{2L^2 b^2 \beta + ae^{-bL}(1 + Lb) - bre - \frac{1}{2}b^2 re^2 - 1}{4L^2 b^2 \beta}\right)\left(\frac{\eta}{\nu}\right) - \frac{1}{\nu} \tag{30}$$

The expressions of transverse shears in Eqn.'s (28) and (30) for various loading conditions are plotted in Fig. 8- Fig. 10.
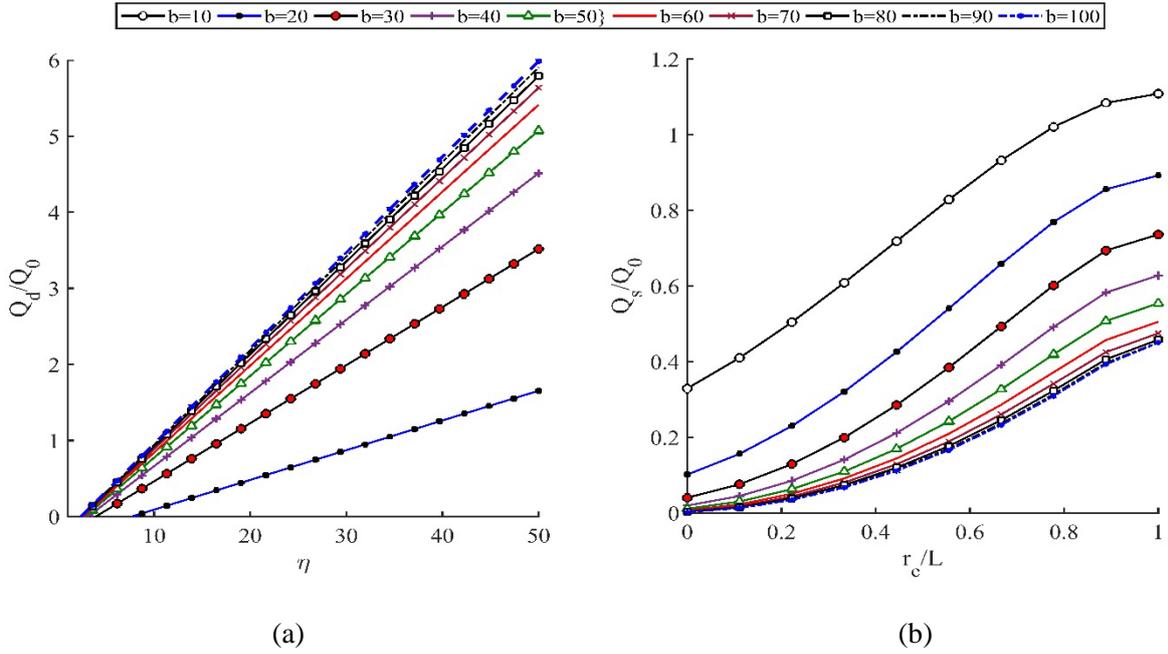
Fig. 8-(a) Influence of the Loading parameters on the dynamic transverse shear at the plate contour. With $H/L = 0.3$ and $r_e/L = 0.12$ (b) Static transverse shear effect with various loading type- with $H/L = 0.02$

1
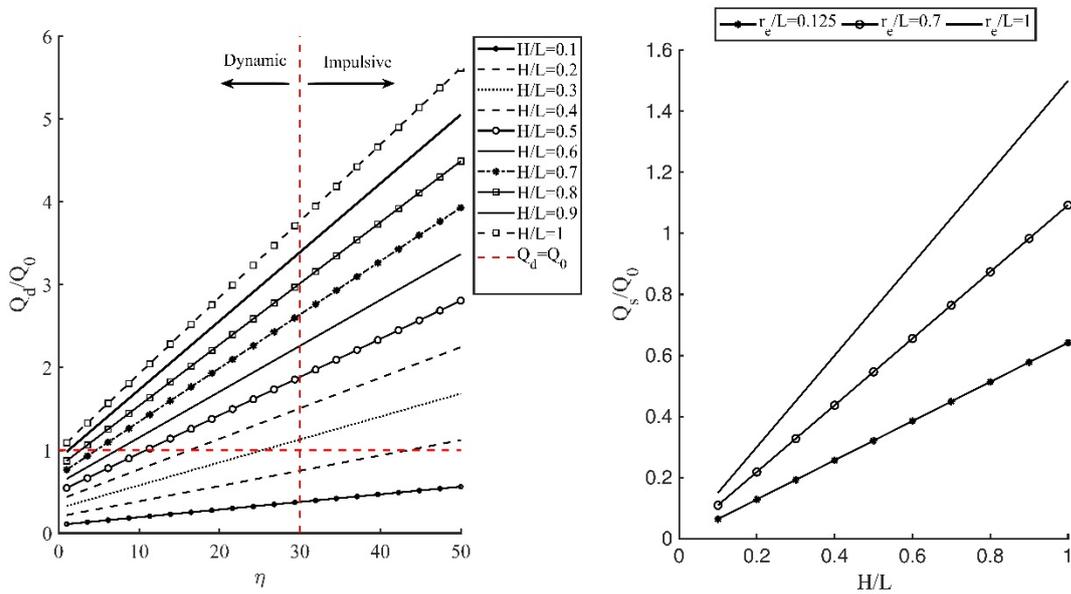
Fig. 9-Influence of the overloading factor on the dynamic transverse shear ($r_e/L = 0.7$) ($b = 50$)

Fig. 10-Influence of the thickness on the static transverse shear ($b = 50$)

2

3   It is evident from Fig. 8 and Fig. 9 that when $H/L \ll 1$, the transverse shear deformations under

4   static loads are infinitesimal compared to the bending deformations and do not contribute to the overall

5   response. The contribution of the transverse shear forces decreases as the loading is targeted to the

6   localised portion at the plate centre, i.e., $r_e/L \ll 1$, which is the typical case of the localised blasts (Fig.

1   10) . Notwithstanding this, the dynamic shear sliding is intrinsically influenced by the load amplification

2   factor η. As the magnitude of η increases to values more than 30, the loading attribute can be idealised

3   as impulsive, giving rise to considerable shear sliding (Fig. 9) even for plates of moderate thickness

4   (e.g. H/L=0.3 or $\nu = 3.3$). Transverse shear effects for moderate values of η are important only for very

5   stocky plates which do not constitute practical cases in the design of protective systems.

6

7   **4.1   Impulsive loading of Class I (very stocky) plates ($\nu \leq 3/2$)**

8   In the case of very stocky plates, it may be assumed that the plate would take the form of Fig. 11.

9   The plate is weak under the shear and the velocity profile is dominantly characterised by the shear

10   sliding at both ends. Subsequently, from Eqn. (12), $f = \mu\ddot{W}/6$ (since $I_r = p_0 = 0$) and Eqn. (15) may

11   be re-written as:

$$\ddot{W} = \frac{-2Q_0}{\mu L} \tag{31}$$

12   since at $x = L$ (or $y = L$), $Q = -Q_0$. Integration of Eqn. (31) twice, together with imposition of initial

13   conditions of $W(0) = \dot{W}(0) = 0$, yields:
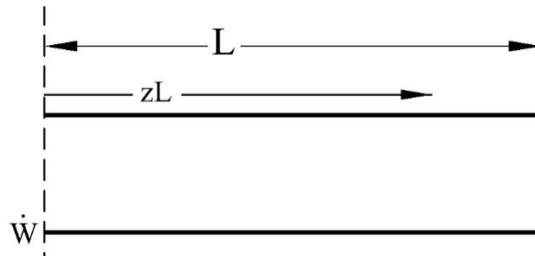
Fig. 11-velocity profile of very stocky plates

14
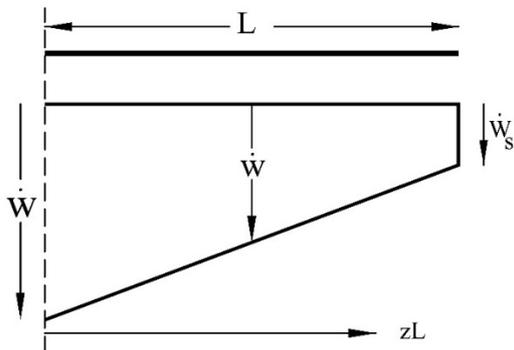
Fig. 12- The assumed velocity profile-phase 1   **Fig.13- The assumed velocity profile-phase 2**
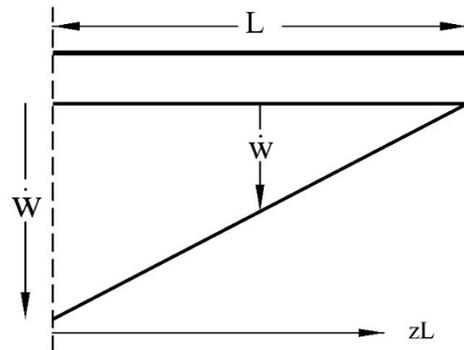
15

$$W(t) = \frac{-Q_0}{L\mu} t^2 + V_1 t \tag{32}$$

The plate comes to rest at $T = \frac{V_1 L \mu}{2Q_0}$, corresponding to the terminal permanent deflection of:

$$\bar{w}_f = \frac{\bar{\lambda}}{8v} \tag{33}$$

Thus, the principle moment in Eqn. (14) may be expressed as:

$$\bar{m} = 1 - \frac{2vz^2}{3} \tag{34}$$

This expressions satisfies the static admissibilty provided $v \leq 1.5$. When $v > 1.5$, Eqn. (34) violates the yield condition, as the moment penetrates the yield surface. The yield violation requires an alternative velocity profile to be assumed, described as follows.

4.2 Impulsive loading of Class II (stocky) plates, $(1.5 < v \leq 2)$

It may be assumed that for $v > 1.5$ the motion is characterised in two distinct phases. The first phase of motion is governed by incipient velocity discontinuity at the support due to the infinite shear sliding, as presented in Fig. 12. The velocity profile in this phase is expressed as $\dot{w} = \dot{W}_s + (\dot{W} - \dot{W}_s)(1 - z)$. In the second phase of motion, the velocity profile ultimately develops into that of Fig.13, as the velocity discontinuity at the plate supports due to the transverse shear sliding vanishes. Thus, the moment function can be written as in Eqn.'s (35) and (36). It turns out that $A_1 = B_1 = 0$ to satisfy the admissibility of stress fields at the plate centre $Q_x|_{z=0} = 0$, while the continuity of the stress fields to the right and left of the load radius i.e. $Q_x|_{z=+r_e/L} = Q_x|_{z=-r_e/L}$ further leads to $D_1 = E_1 = 0$ for the impulsive load types. Thus, the moment function is characterised by the inertia effects as:

$$f = \begin{cases} \dfrac{\left(\mu\left((\ddot{W} - \ddot{W}_s)(2 - z) + 2\ddot{W}_s\right) - p_0\right)}{12} + \dfrac{A_1}{z^2} + \dfrac{B_1}{z^3} & 0 \leq z \leq r_e/L \quad (35) \\[4mm] \dfrac{-ap_0 e^{-bLz}(bLz + 2)}{(bLz)^3} + \dfrac{\mu\left((\ddot{W} - \ddot{W}_s)(2 - z) + 2\ddot{W}_s\right)}{12} + \dfrac{D_1}{z^2} + \dfrac{E_1}{z^3} & r_e/L \leq z \leq 1 \quad (36) \end{cases}$$

In the same spirit, from $Q_x(x = L, y = 0) = -Q_0$ and $M_2(z = 1) = 0$ at the plate periphery, two sets of expressions are ensued and solved simultaneously to furnish the inertia terms as in Eqn.'s (37)-(39).

$$\ddot{W} = -\frac{12M_0(2 - v)}{L^2 \mu} \tag{37}$$

$$W = V_1 t - \frac{6M_0 t^2(2 - v)}{L^2 \mu} \tag{38}$$

$$\ddot{W}_s = \frac{12 M_0 (1 - v)}{L^2 \mu} \tag{39}$$

1   This phase terminates when the velocity discontinuity vanishes at the support ($\dot{W}_s = 0$), which
2   occurs at $t = T_1$, given by Eqn. (40). The dimensionless permanent maximum deformation associated
3   with this time is given in Eqn. (41):

$$T_1 = \frac{L^2 V_1 \mu}{12 M_0 (v - 1)} \tag{40}$$

$$\frac{W_1}{H} = \frac{\bar{\lambda}(3v - 4)}{24\,(v - 1)^2} \tag{41}$$

4   Evaluating the bending moment by Eqn. (34) with inertia term now known *a priori*, yields the
5   moment at any point in the plate:

$$\bar{m} = -(z - 1)(z + 2vz^2 - 3z^2 + 1) \tag{42}$$

6   At the plate centre, the range of $v > 2$ causes a yield violation ($\partial^2 \bar{m}/\partial z^2 > 0$). Consequently, the
7   profile assumed in this phase remains valid for the range of $1.5 < v \le 2$ only.

8   **4.2.1   Second phase of motion**

9   The time derivative of Eqn. (38) suggests a reserved kinetic energy in the plate which must be dissipated
10   before the motion ceases. Since the shear sliding vanishes at T_1, the velocity profile would furnish to
11   $\dot{w} = \dot{W}(1 - z)$; which reduces the P.D.E's given in Eqn.'s (12) and (13) to Eqn.'s (35) and (36) but
12   with $\ddot{W}_s = 0$. Thus, evaluating the simply supported boundary condition of moment (i.e. $\bar{m} = 0$) gives
13   $\ddot{W} = -12M_0/L^2\mu$, whereby the corresponding transverse velocity field is given by:

$$\dot{W}_2 = 2V_1 - 12M_0 t/L^2 \mu \tag{43}$$

$$W_2 = V_1 \left[2t + \frac{\tau^*}{24(1 - v)} - \frac{6t^2}{\tau^*} \right] \tag{44}$$

14   The succeeding Eqn.'s (43)-(44) are attained by ensuring the kinematic continuities of velocity and
15   transverse displacement fields with the previous phase at $t = T_1$. The motion terminates at $t = \tau^*/6$,
16   which gives the permanent transverse displacement as:

$$\bar{w}_f = \frac{\bar{\lambda}(4v - 5)}{24(v - 1)} \tag{45}$$

17

15

4.3 Class III plates ($v > 2$)

4.3.1 Phase 1- $0 < t < T_1$

Clearly, the foregoing velocity profile causes a yield violation at the centre when $v > 2$, suggesting a modification to the velocity profile for this class of plates. It transpires that the velocity profile is characterised with three stages of motion, namely, (i) phase 1 with appearance of incipient stationary plastic hinge in Fig. 14, (ii) phase 2 where the plastic hinge travels inward (Fig. 15) and (iii) phase 3 with the residual deformation as the central plastic hinge zone disappears, in which the velocity profile develops from that of Fig. 15 to Fig.13. Thus, in the first phase of motion, the velocity profile may be assumed as

$$\dot{w} = \dot{W} \qquad\qquad \mathbf{0 \leq z \leq \xi_0} \qquad (46)$$

$$\dot{w} = \frac{(\dot{W} - \dot{W}_s)(1 - z)}{1 - \xi_0} + \dot{W}_s \qquad\qquad \mathbf{0 \leq z \leq r_e/L} \qquad (47)$$

which furnishes the succeeding moment function to:

$$
f = \begin{cases}
\left(\mu\ddot{W} - p_0\right)/6 + A_3/z^2 + B_3/z^3 & 0 \leq z \leq r_e/L & (48) \\[2mm]
\dfrac{\mu\ddot{W}}{6} - \dfrac{ap_0 e^{-bLz}(bLz + 2)}{(bLz)^3} + D_3/z^2 + E_3/z^3 & r_e/\mathrm{L} \leq z \leq \xi_0 & (49) \\[4mm]
\dfrac{-ap_0 e^{-bLz}(bLz + 2)}{(bLz)^3} + \dfrac{\mu\left(\dfrac{(\ddot{W}_1 - \ddot{W}_s)(2 - z)}{1 - \xi_0} + 2\ddot{W}_s\right)}{12} + \dfrac{F_3}{z^2} + \dfrac{G_3}{z^3} & \xi_0 \leq z \leq 1 & (50)
\end{cases}
$$

It is also assumed that $\xi_0 \leq r_e$. The yield condition of the bending moment in the central zone gives $\bar{m} = 1$; thus, $Q = 0$ and $\mu\ddot{W} = p_0$ throughout the entire central zone $0 \leq z \leq \xi_0$, which when integrated twice with respect to time gives $\dot{W}_1 = p_0 t/\mu$ and $W_1 = p_0 t^2/2\mu$, respectively. The constants of the piecewise moment function in this zone are obtained by ensuring the continuity of the transverse shear and bending moment at $z = r_e/L$ and at the plate centre; they are accordingly identical to Eqn. (24a), whereas the O.D.E constants in (50) may be evaluated from the kinematic conditions of f at $z = \xi_0$, (i.e. $Q = 0$ and $\bar{m} = 1$) as:

$$F_3 = \frac{\left(-6a(\xi_0 - 1)(Lb\xi_0 + 1)e^{-Lb\xi_0} - (bL\xi_0)^2(2\xi_0 - 3)\right)p_0}{6L^2 b^2(\xi_0 - 1)} - \frac{\ddot{W}_s \mu \xi_0^3}{6(\xi_0 - 1)} \qquad (51)$$

$$G_3 = \frac{\left[(3\xi_0 - 4)(bL\xi_0)^3 + 12a(\xi_0 - 1)((bL\xi_0)^2 + 2Lb\xi_0 + 2)e^{-Lb\xi_0}\right]p_0}{12L^3 b^3(\xi_0 - 1)} + \frac{\ddot{W}_s \mu \xi_0^4}{12(\xi_0 - 1)} \qquad (52)$$

1
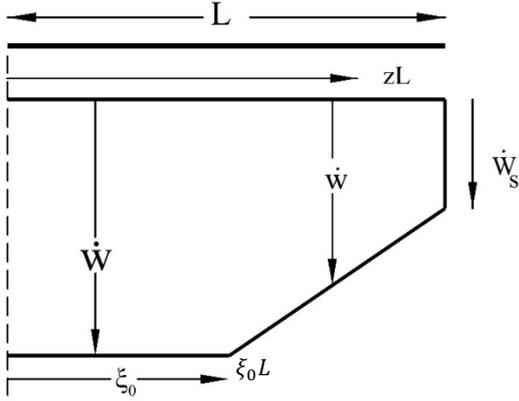
Fig. 14- the assumed velocity profile for plates of $\nu > 2$ at first phase of motion
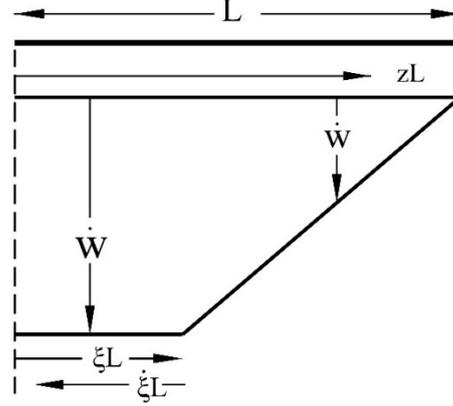
Fig. 15- assumed velocity profile for plates of $\nu > 2$ at subsequent phase of motion

2 Substituting Eqn.'s (47)-(49) in (14)-(16), and enforcing the boundary conditions of $Q_x = -Q_0$ and

3 $M_1 = 0$ at $x = L$ yields two sets of expressions, the former is used to evaluate the inertia at the support

4 $\ddot{W}_s$ in Eqn. (53). Thus, we have:

$$\ddot{W}_s = \left[\frac{-\delta p_0}{M_0 b^2 (\xi_0^2 + \xi_0 - 2)} + \frac{12\nu}{(\xi_0^2 + \xi_0 - 2)} \right] \ddot{\bar{w}}$$

(53)

5 where $\ddot{\bar{w}} = V_1 / \tau^*$ and δ is given by:

$$\delta = -6a(Lb\xi_0 + 1)e^{-Lb\xi_0} + 6a(Lb + 1)e^{-bL} - 2b^2 L^2 (\xi_0 + 1/2)(\xi_0 - 1)$$

(54)

6 The latter condition is used to evaluate an expression of the stationary plastic hinge ξ_0 in Eqn. (55)

$$\bar{m} = \frac{\Gamma \eta}{12 L^3 b^3 \beta} + \frac{\mu L^2 (\xi_0 + 1)(\xi_0 - 1)^2 \ddot{W}_s}{12 M_0} + 1 = 0$$

(55)

7 where

$$\Gamma = 12a \left(2 + b^2 L^2 \xi_0 (\xi_0 - 1) + bL(2\xi_0 - 1) \right) e^{-Lb\xi_0} - 12a(Lb + 2)e^{-Lb}$$
$$+ L^3 b^3 (3\xi_0 + 1)(\xi_0 - 1)^2$$

(56)

8 The expression of ξ_0 in Eqn. (55) is highly nonlinear which may either be solved by numerical

9 methods, or, alternatively, by truncation of the exponential term $e^{-Lb\xi_0}$ into sum of polynomials, using

10 the Taylor expansion. It should be noted that, in the absence of the inertia term $\ddot{W}_s$, corresponding to

11 when ν becomes large, the expression (55) converges to that of plates under bending only.

Eqn. (53) is similar to the analyses of [13], [16] except with an additional coefficients of load appearing in the first term in the bracket, due to the spatial distribution of the localised blast load. A time integration of (53) yields:

$$\dot{W}_s = \left[\frac{-\delta p_0 \tau}{M_0 b^2 (\xi_0^2 + \xi_0 - 2)} + \frac{12 v t}{(\xi_0^2 + \xi_0 - 2)} \right] \ddot{\bar{w}} \qquad (57)$$

This phase terminates when the velocity discontinuity due to shear sliding at the support vanishes, at time T_1 given by Eqn. (58):

$$T_1 = \frac{\delta p_0 \tau}{12 b^2 M_0 v} \qquad (58)$$

The permanent displacement corresponding to this time is given as:

$$\frac{W_1}{H} = \frac{\delta^2 p_0^3 \tau^2}{288 M_0^2 b^4 v^2 \mu H} \qquad (59)$$

In the case of impulsive loads, $\ddot{W} = p_0 = 0$ and only the last terms on the right-hand side of the expressions (51)-(52) remains non-zero. In such a case, the expression of transverse deformation at the discontinuity front simplifies to $W_s = V_1 t + (6 V_1 v t^2)/(\tau^* (\xi_0^2 + \xi_0 - 2))$. Thus, the end time of this phase can be evaluated as $T_1 = \tau^*/12(2 - \xi_0^2 - \xi_0)$, which furnishes the permanent deformation to Eqn. (60)

$$\frac{W_1}{H} = \frac{\bar{\lambda}}{12[2 - \xi_0^2 - \xi_0]} \qquad (60)$$

which is similar to the results obtained for impulsively loaded circular plates in Ref. [14], except the spatial distribution of the load contributes to the magnitude of the impulsive velocity V_1, and by extension, the dimensionless kinetic energy. The plastic bending moment and shear force in the outer zone of the (impulsively loaded) plate may be written as:

$$\bar{m} = 1 - \frac{\ddot{W}_s (\xi_0 + z)(\xi_0 - z)^3}{12 \ddot{\bar{w}} z (1 - \xi_0)} \qquad \xi_0 \le z \le 1 \qquad (61)$$

$$Q_x = \frac{\mu x \ddot{W}_s (\xi_0 - z)^2 (\xi_0 + 2z)}{6 z^2 (1 - \xi_0)} \qquad \xi_0 \le z \le 1 \qquad (62)$$

Since M is continuous at the plastic bending hinge (i.e. $M_x = M_0$ at $x = \xi_0 L$ and $y = 0$, or $M_1 = M_0$ at $z = \xi_0$), the position of the initial plastic hinge would be delineated in Eqn. (63) and illustrated in Fig. 16 as a function of plate's non-dimensional thickness parameter v.

$$\xi_0 = \frac{(-1 + \sqrt{4v^2 - 8v + 1})}{2v} \tag{63}$$

1
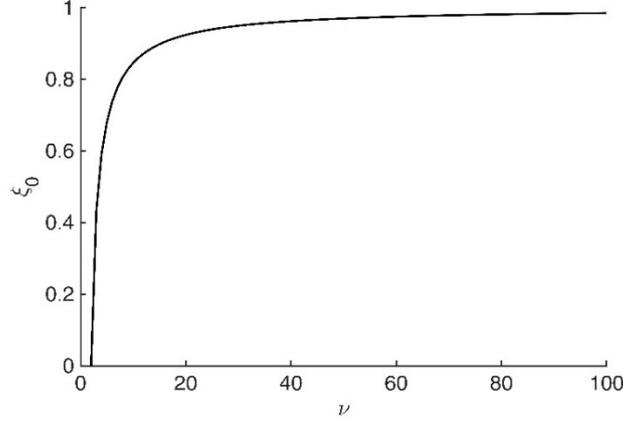
Fig. 16-variation of ξ_0 with v

2

3 **4.3.2 Phase 2- $T_1 < t < T_2$**

4   Following the first phase of motion, the transverse shear sliding is removed at the supports at the

5 onset of this phase $t = T_1$, and the deformation assumes the profile in Fig. 15. It may be assumed that

6 the central zone travels with constant velocity $\dot{W}_2$, while the plastic hinge $\xi(t)$ now moves inward

7 toward the centre of the plate. Thus, clearly $\ddot{W} = 0$, and the kinematic admissibility dictates that $\dot{W}_2 =$

8 $\dot{W}_1$ at $t = T_1$, leading to $\dot{W}_2 = p_0 T_1/\mu$. The constants of moment function are determined as:

$$F_3 = \frac{\mu \xi^2 \dot{W} \dot{\xi}(2\xi - 3)}{6(\xi - 1)^2} \tag{64}$$

$$G_3 = -\frac{\mu \xi^3 \dot{W} \dot{\xi}(\xi - 4/3)}{4(\xi - 1)^2} \tag{65}$$

9 which are obtained by substitution of $\ddot{w} = (1 - z)d(\dot{W}/(1 - \xi(t)))/dt$ in Eqn.'s (12)-(13), using

10 $p_0 = 0$ and solving the P.D.E.

11   By appreciating the boundary condition of the principle moment at the edge, (i.e. $M_2|_{z=1} = 0$), an

12 expression of the travelling plastic hinge is obtained:

$$\bar{m} = 1 - \frac{1}{4}\tau^* \dot{\xi}(t)\left(\xi(t) + \frac{1}{3}\right)(\xi(t) - 1) = 0 \tag{66}$$

13 By integrating Eqn. (66) the position of travelling plastic hinge can be delineated by Eqn. (67)

$$t + \frac{\tau^* \xi(t)(\xi(t)^2 - \xi(t) - 1)}{12 M_0} = \tau^* \tag{67}$$

19

where the constant of integration is obtained from the kinematic conditions, i.e. $\xi(t = T_1) = \xi_0$. The size of the central plastic zone decreases monotonically and ultimately vanishes as the plastic hinge $\xi(t)$ reaches the centre of the plate, i.e. $\xi(t) = 0$. This marks the end of phase 2 which occurs at time $t = T_2$, given as:

$$T_2 = \frac{\tau \delta p_0 [p_0 L^2 \xi_0 (1 + \xi_0 - \xi_0^2) + 12 M_0)}{144 M_0^2 b^2 \nu} \tag{68}$$

which is simplified to $T_2 = \tau^*/12$ for the impulsive loading case.

4.3.3   Phase 3 $T_2 \leq t \leq T_f$

The central plastic hinge disappears at $t = T_2$. However, the plate contains reserved kinetic energy which must be dissipated before the plate finally comes to rest. Therefore, the motion continues with residual deformation, however, the velocity profile is characterised by a conical velocity which is identical to that of the previous case, i.e. the profile given in Fig.13.

The inertia term of such conical profile, expressed by $\ddot{W}_3 = -12\overline{\ddot{w}}$, may be evaluated by the same procedure in section 4.2, but with shear sliding inertia and pressure term is eliminated from Eqn.'s (35)-(36) and considering dynamic loads. The solutions to the permanent deformation and velocity fields at this phase are achieved by time integration of the inertia term $\ddot{W}_3$, in addition to employing the kinematic admissibility conditions of the velocity and deformation fields with the phase 2 of deformation. The final displacement can be recovered when the velocity vanishes, (i.e. $\dot{W}_3$=0):

$$W_f = \frac{p_c \left(\frac{\eta}{\beta} \left(-\xi_0^3 + \xi_0^2 + \xi_0 + \frac{1}{2} \right) + 6 \right)}{1728 \mu \eta} \left(\frac{\delta \tau \eta p_0}{\nu M_0 b^2} \right)^2 \tag{69}$$

In the case of impulsive loads, the inertia term is identical to Eqn. (37) and the deformation fields are furnished as per Eqn.'s (70) and (71).

$$\frac{W_3}{H} = \frac{2 V_1 t}{H} - \frac{\bar{\lambda}}{24} - \frac{6 V_1 t^2}{\tau^* H} \tag{70}$$

$$\dot{W}_3 = 2 V_0 - \frac{12 M_0 t}{L^2 \mu} \tag{71}$$

In such a phenomenon, the theoretical procedure leads to $\bar{w}_f = \bar{\lambda}/8$, a similar expression to the results of [1] for circular plates, while $\bar{\lambda}$ is influenced by the loading distribution. The permanent deformation in the case of impulsive load would occur at $T_f = \tau^*/6$.

Provided the transverse shear strain does not contribute to the deformation gradients, i.e. the shear sliding at the support vanishes, the end time of first phase of motion T_1 from Eqn. (58) occurs at $T_1 = \tau$,

1 further reducing the terms of the Eqn. (69) to the solution of plates where the shear sliding along the

2 plate periphery is absent and the plastic flow may be characterised by the interactive yield curve of

3 bending moments, only. The central and end-point permanent deformations of the plate for various

4 values of ω_0 and ν are plotted in Fig. 17 and Fig. 18, while the combined influence of the load magnitude

5 and the plate thickness (based on ν) are graphed in Fig. 19.
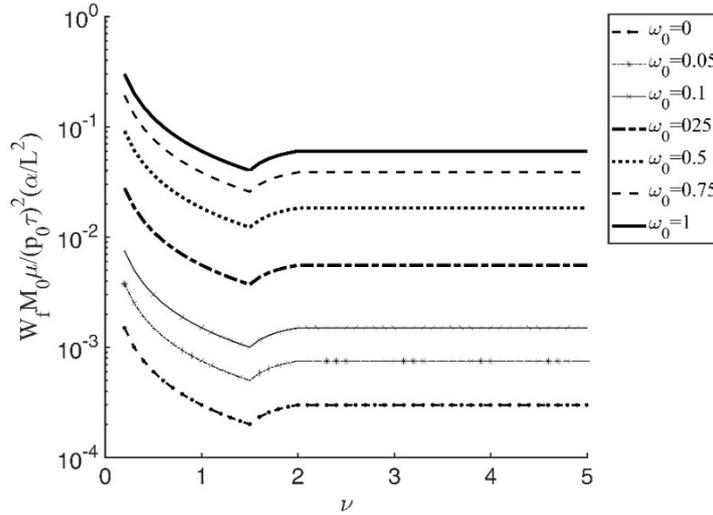
Fig. 17- Variation of the central permanent deflection (W_f) with
ν for various loading conditions of impulsive load, where $\omega_0 =$
r_e/L

6
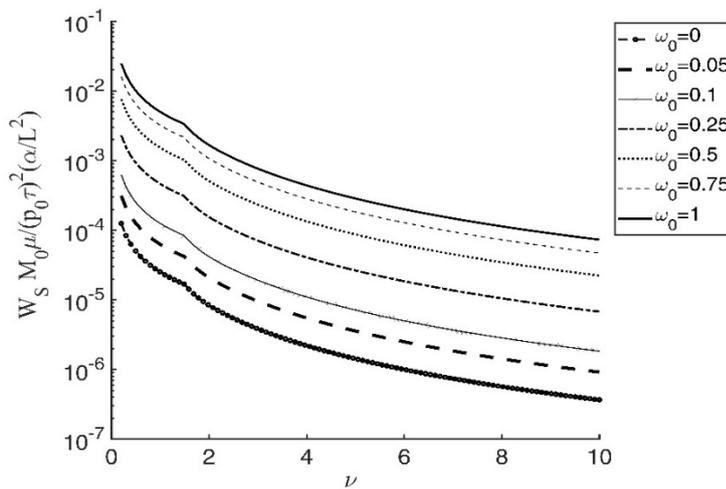
Fig. 18- Variation of the deformation profile at discontinuous front
(W_s) against ν for various impulsive blast loading radii

7

8
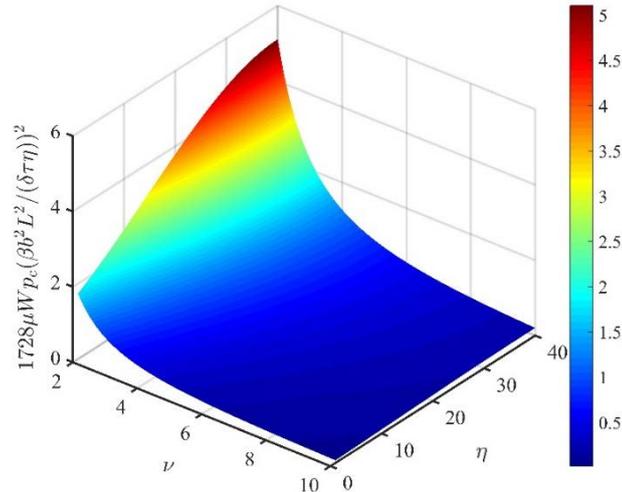
Fig. 19- Interaction surface of the plate thickness and dynamic load amplification factor on the central deformation (for interpretation of colour in this figure, the reader is referred to the online version)

4.4 Fully clamped plates

The foregoing analyses on the simply supported plate systems may be extended to the case of fully-clamped plate. Considering the boundary condition of principle moment at the plate contours, $\bar{m} = -1$, resulting in the static plastic collapse at $p_{cl} = 2M_0/(\beta L^2)$. Thus, the expressions in each class of fully clamped plates may be obtained by merely replacing M_0 with $2M_0$, η with $\bar{\eta} = \eta/2$ and v with $\bar{v} = 1/2 \, v$ in the expressions of permanent deformations for each class of plates, without the need for further analysis. The classification of the plates, in accordance of the range of slenderness ratio, is modified to:

- Class I plates $\bar{v} < 3$
- Class II plates $3 < \bar{v} < 4$
- Class III plates $4 < \bar{v}$

5 Finite Element simulations

The analytical solutions of class III simply supported and clamped plates are validated against full 3D numerical models in Finite Element commercial software ABAQUS® Explicit. Due to axisymmetric nature of the load, only a quarter of the plate was considered in each model with symmetry boundary conditions.

The parametric validations were carried out in two categories. The first category FE models were investigated in the pure Lagrangian reference frame, whereas in the second category, the blast phenomenon was simulated using an Eulerian reference frame, whose associated continuum mechanics algorithms were coupled with those of Lagrangian analysis, commonly referred to as the Multi-Material Arbitrary Lagrangian Eulerian, and consisted of the Uncoupled Eulerian Lagrangian (UEL) with rigid

22

1   target, as well Coupled Eulerian Lagrangian (CEL) with deformable target. The UEL analyses were

2   performed as preliminary to delineate the load parameters for the sake of theoretical input. Full details

3   of the MMALE analysis and the material models are discussed elsewhere [32]–[35], but a brief

4   description is given hereunder.

5   The target plate was assumed of either austenitic Mild steel (for the pure Lagrangian model) or

6   ultra-hard armour steel alloy AR440T from [36] (re. the CEL models), each prescribed a density of

7   7850kgm[-3], Young modulus of 200GPa and characteristic in-plane lengths of 400×400mm, thicknesses

8   of 60mm (Mild steel) and 10mm (armour steel), with modified Ramberg-Osgood material model which

9   was idealised as elastic-perfectly plastic. The visco-plasticity phenomenon was disregarded as armour

10 steel material are impervious to the strain rate up to $3000 s^{-1}$ [37]. However, the flow stress was taken

11 as the average of yield stress and ultimate tensile stress to approximate the influence of strain hardening.

12 The values of 330MPa and 1342MPa were chosen for Mild steel (M.S) and armour steel (AR)

13 respectively.

14   The panels were discretised with a mesh of four node S4R elements, with finite membrane strains,

15 elemental length of 4mm to satisfy mesh convergence. The S4R elements are of general purpose

16 conventional shells with reduced integration formulation and hourglass control to prevent shear locking.

17 These elements are compatible with thick plate's formulations.

5.1 Pure Lagrangian method

19   In the pure Lagrangian analysis, the mesh follows the material movement. The pure Lagrangian

20 methods offer simplicity and reduced computational time due to the simplified description of the blast

21 load. For blast assessment of proximal loads, the numerical calculations should be couched in caveats

22 on the accuracy due to the complexity of the fluid structure interaction phenomenon. Furthermore, the

23 mesh is prone to excessive distortion when treating the fluid mechanic problems. However, while these

24 approaches overestimate the maximum deformations, they are capable of capturing the permanent

25 deformations and pressure time histories of distal charges quite well [33].

26   The loading was described by a FORTRAN coded user defined subroutine VDLOAD in each case

27 of ω_0. To confirm the displacements would be in the outset of elasticity, the equivalent plastic strain

28 ($\bar{\varepsilon}_p$) was monitored to ascertain that the panels reach the outset of their elasticity.

29   A total of 10 Fe models were set up with constant load magnitude of 2400MPa. The plates had 75

30 points of integration through 60mm thickness while the boundary the target plate was pinned. These

31 panels were subjected to pulse pressure load of various central uniform load radii but constant load

32 exponent of $b = 100 m^{-1}$. The temporal shape of the load was assumed with a rectangular pulse with

33 the duration of $\tau = 30 \mu s$.

5.2 Multi-Material Arbitrary Lagrangian Eulerian method

The CEL models are part of the Arbitrary Lagrangian Eulerian formulations to simulate the blast phenomenon considering the Fluid-Structure Interaction (FSI). In the CEL analysis, the detonated explosive products flow through the mesh points of the reference frame-which is fixed in space. The state variables are then transferred through the mesh by using the second advection method [38]. Upon contact with the structure, the FSI algorithms are invoked at the contact interface of the target and explosive products (which are assumed to interact in a frictionless manner) to characterise the motion of the target.

The multi-material (for a free air blast) in this study, consisted of air and explosive, were embedded in an Eulerian cuboid of 300 mm length. The medium was discretised with EC3D8R Eulerian brick elements in ascending lengths of 3mm at the region of interest in the vicinity of the charge to 8mm at the transmission boundaries. The transmission boundaries were assigned with flow-out boundary conditions, while the other faces were adjusted with symmetric boundaries (Fig. 20 (a)). In Fig. 20 (b) the schematic of the CEL model is presented.

Fig. 20 illustrates the preliminary UEL models. A total of four FE models were set up with Plastic Explosive 4 (PE4) cylindrical sheet explosive of density $1.601 g.cm^{-3}$, designated charge diameter $D_e = [50, 75, 100, 140]$ at constant 50mm stand-off from the target. The height of 70g charge ($D_e = 50$mm) was 22.28mm, while the charge mass of the rest was varied to yield a constant height of 5.57mm. The clamps were specified with 10mm rigid chamfers at the edge of the target, to account for the clamps contribution in absorption of a portion of the impulse generated by the explosive. The reduction of transmitted impulse to the target is brought about by the increased charge radius to plate length ratio [39].

Table 1- load parameters from the FSI model

Design number	1	2	3	4
$D_e(mm)$	50	75	100	140
$H(mm)$	10	10	10, 20	20
$M_e(g)$	70.0	39.4	70.0	137.3
$p_0\ (MPa)$	1500	440	680	732
$r_e(mm)$	18.4	22.4	36.9	57.3
$b(\mathrm{m}^{-1})$	79.4	80.0	57.8	48.7

The pressure registered with each target gauge point was recorded and plotted in Fig. 21-Fig. 23, while Table 1 shows the charge properties and loading conditions. It turns out that with the increase of charge diameter, r_e increases while b decreases. The variation of the state parameters are rather smooth provided the quotient of stand-off to charge diameter exceeds 1.5 [40], [41].

24
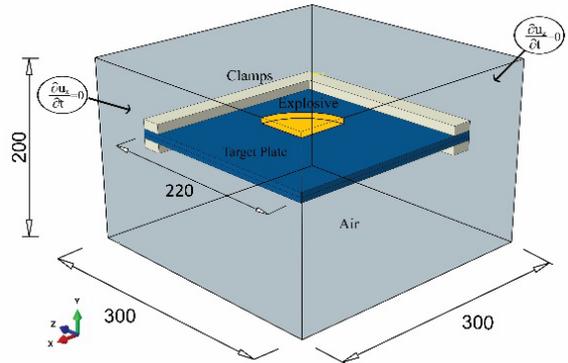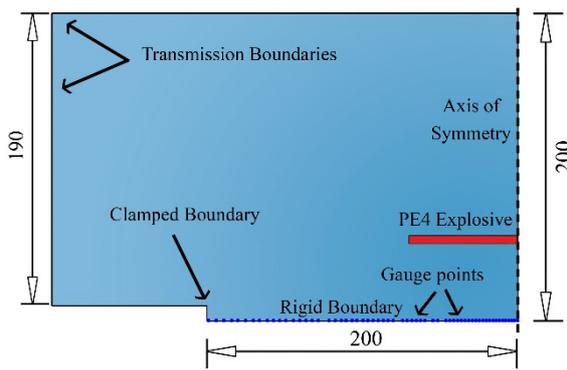
(a)   (b)

Fig. 20- The schematic of the FE model with rigid target (a) Deformable target plate (b)- units in mm

1
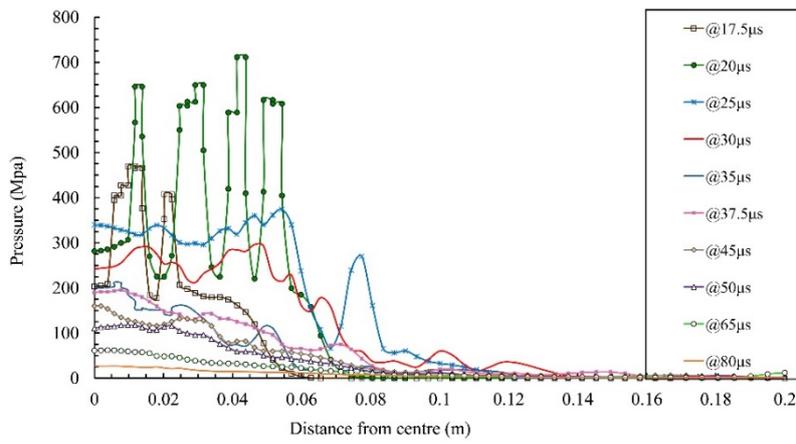
**Fig. 21- Recorded pressure at gauge points vs distance from the target -
140mm PE4 explosive**

2
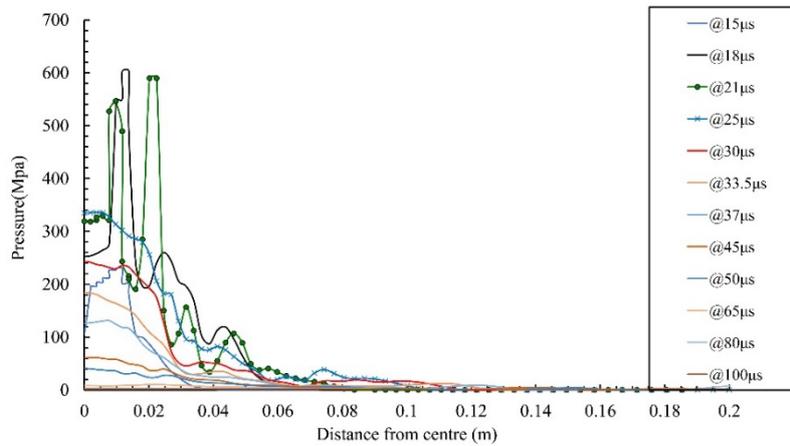
**Fig. 22 Recorded pressure at gauge points vs distance from the target -75
mm PE4 explosive**

1
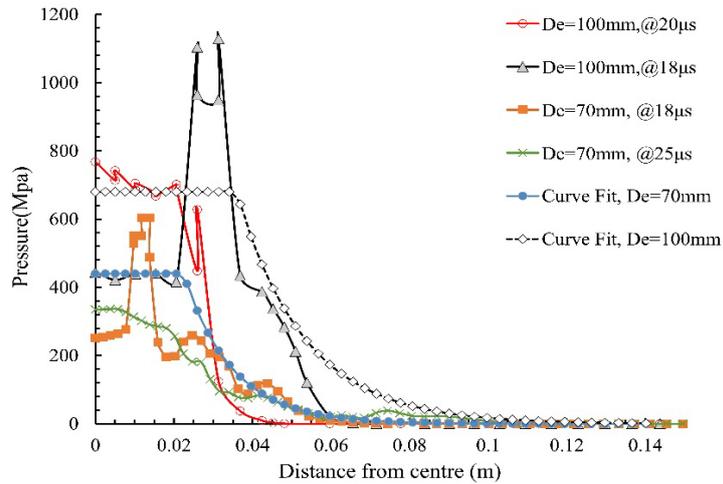
Fig. 23 Curve fit of the spatial distribution of the blast for 75mm and 100mm charge diameters

2

3   The FE models were then designed as deformable targets (referred to as the CEL models) and

4   fixated with two upper and lower clamps along their periphery, as illustrated in Fig. 20 (b). The design

5   number 4 (with the 10mm target plate) underwent excessive distortion and was disregarded from the

6   results, thus two further panels of 20mm thickness were investigated instead. The detonation was

7   assumed to initiate from the centre of the explosive. The air and explosive material models were

8   described as Ideal gas law and Jones-Wilkins-Lee equation of state, respectively. The reader is referred

9   to the [32] for full details of the FE method and materials.

10   **5.3   Discussions**

11   The position of the plastic hinge ξ_0 in beams and plates may be monitored numerically by tracing

12   the maximum equivalent plastic strain $(\overline{\varepsilon_p})$ that appears instantaneously at the onset of loading. The

13   distribution equivalent plastic strain, transient displacement and Mises stress fields at various times are

14   illustrated in Fig. 24 -Fig. 25. As predicted, the size of central plastic zone broadens with the increase

15   of load radius in the FE models, which corroborates well with the analytical results. The numerical

16   results in Fig. 26 (a) and (b) compare favourably with those of the analytical model. The pure

17   Lagrangian results also reveal the assumed velocity profile predicts the permanent deformation with

18   reasonable accuracy, with error less than 17% in for most loading radii (Fig. 26 a).

19   The targets exposed to the explosives of high charge diameter underwent a sharp increase in the

20   registered pressure, underneath (relatively) the tip of the explosive charge, at the time point of $18\mu s$

21   (Fig. 23). At this point, the reflected wave generated from the gaseous material at the centre of explosive,

22   which travelling across the target plate, merges with the Mach stem at the tip of the explosive. This is

associated with the circular charges of high diameter and low height (i.e. design 2-4). The contact interface underneath the tip

Clearly, due to the increased charge height of the design number 1, the wavefront primarily propagated in vertical direction, inducing elevated pressure at the central region (Table 1) which results in the concentrated transfer of energy to a smaller area of the material.

Some differences in prediction of the permanent deformation, particularly those the CEL models presented in Fig. 27, may be due to the influence of material elasticity or estimation of the load parameters (p_0, b) for analytical models. In the case of former, with the increase of the material yield stress, the strain energy stored elastically during the impact would be significant which influences the post-peak behaviour. However, rigidity of the plate increases with the thickness, thus the contribution of the elastic energy to dissipate the potential energy of the load decreases. Consequently, the system can be idealised as a rigid body in which case the analytical formulations of rigid-perfectly plastic model suffice to predict the response, i.e. the case of 60mm thick panels for pure Lagrangian analysis studied here. Furthermore, it turns out that the parameter r_e has more pronounced effect- compared to b, on the prediction of permanent deformation theoretically [42].

The contribution of elastic strain energy to dissipate the external work reduces the plastic deformations, the case which is pertinent to the armour steel panels. While this reason explains the differences of the predicted deformations in Fig. 27, the phenomenon of localised blast is intrinsically complex process requiring the parameters associated with the fluid structure interaction to be assessed. For example, as the incident pressure impinges transversely upon the middle portion of the target, it is reflected and merges with the wave front of the incident wave, creating a triple point and a Mach stem. The Mach stem travels across the target plate and attenuates before reaching the plate edges. However, a pressure build-up near the supports is also observed, due to the superposition of the reflected wave with the incident wave. The pure Lagrangian models do not account for this phenomenon and may lead to oversimplified, conservative estimate of the full response.

The pressure build-up is more discernible in the models with larger ratio of the explosive diameter to plate full length, i.e. $D_e/2L > 0.25$, in which case, some of the impulse is absorbed by the clamps. Notwithstanding, the pressure build-up is inconsequential to the permanent midspan deformations [39], [43], its effects may be ignored in our validations.
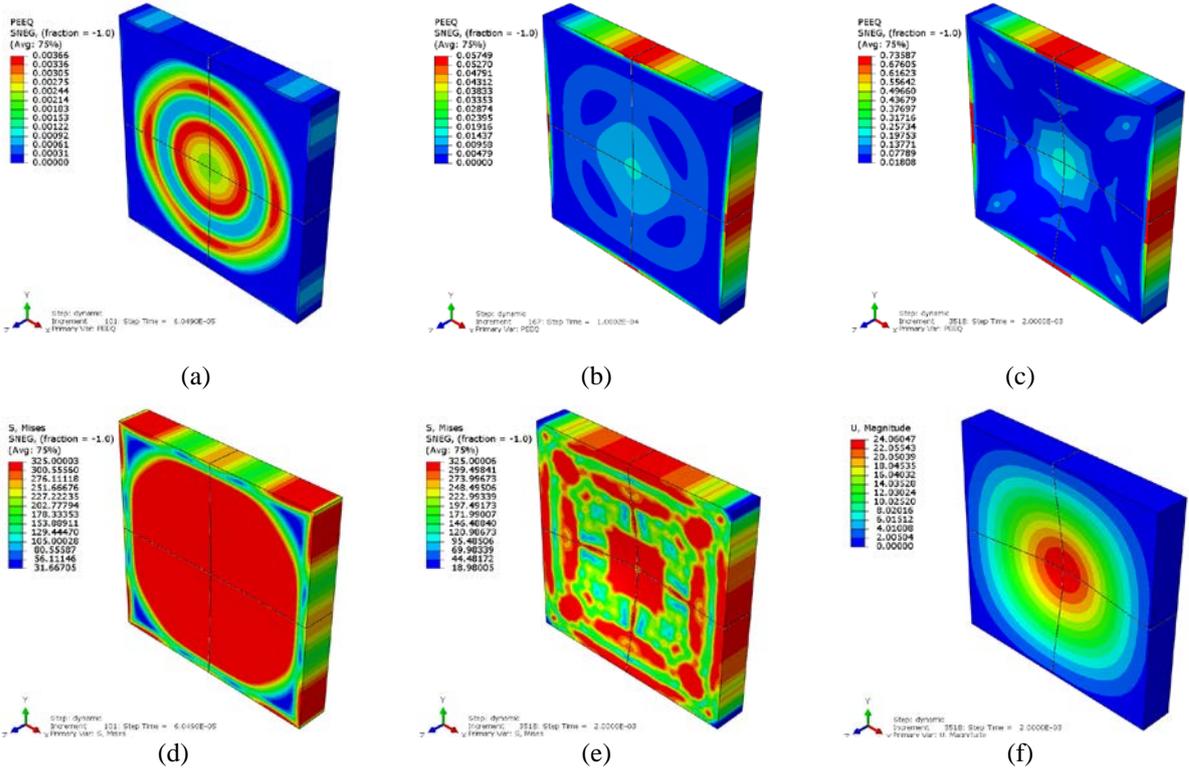
Fig. 24- Distribution of the equivalent plastic strain, von Mises stress and displacement fields in the steel plate with b=100 and $r_e/L = 0.5$. (a-c)- Distribution of $\bar{\varepsilon}_p$ at $t = 60\mu s$, $100\mu s$ and $2ms$, respectively. (d-e) distribution of Mises stress at $t = 60\mu s$ and $2ms$, respectively. (f) permanent displacement at $t = 2ms$
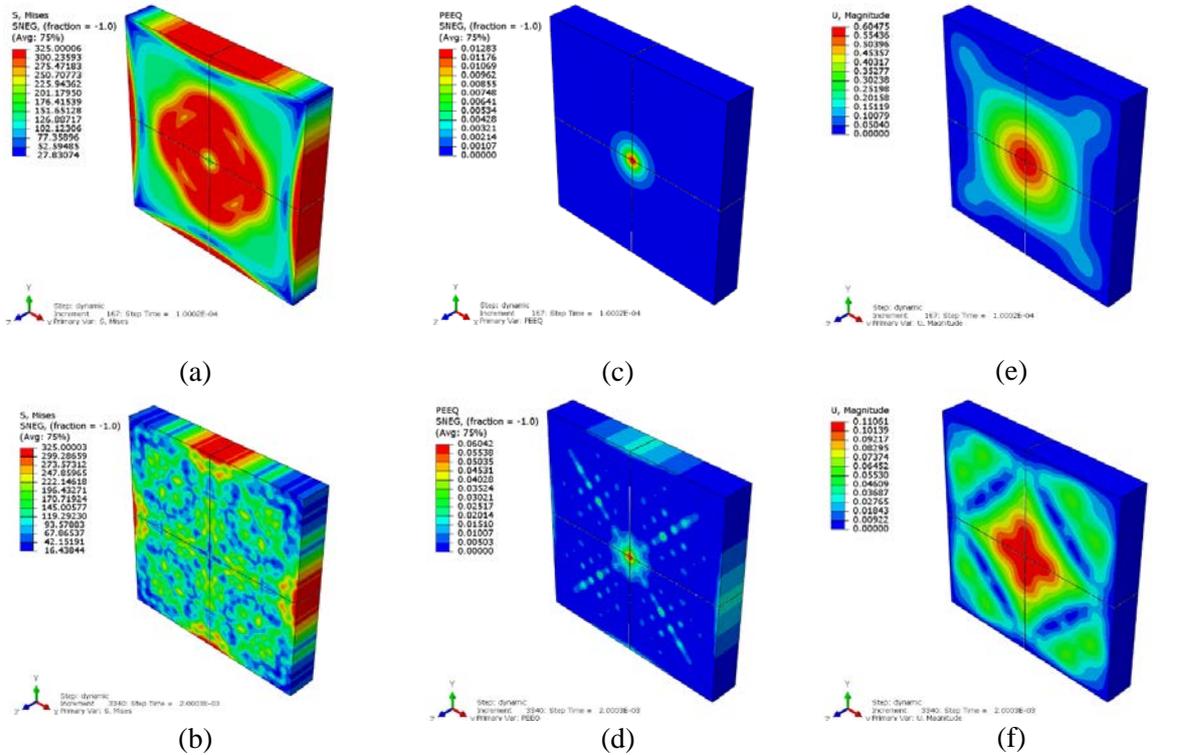
Fig. 25 (a), (b) distribution of the Mises stress; (c), (d) Equivalent plastic strain ($\bar{\varepsilon}_p$); (e), (f) displacement field at $t = 100\mu s$ and $t = 2ms$ in the steel plate with $\nu = 3.\bar{3}$, b=100 and $r_e/L = 0.1$.

In general, the theoretical results concur with the results of CEL models. Clearly, the detonation of sheet explosive ($D_e = 100mm$) is more calamitous than that of the same mass but smaller charge diameter.
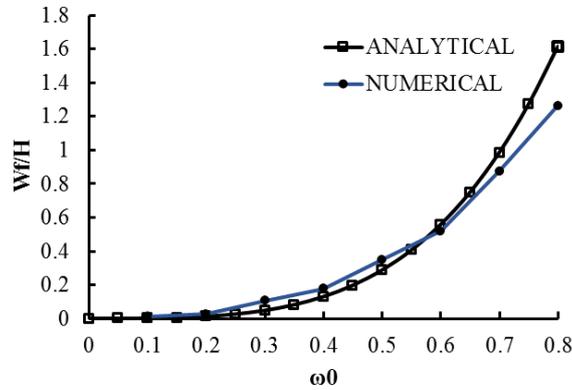
(a)

Fig. 26- Variation of the permanent deformation with load radius, impulsive loading on steel plate
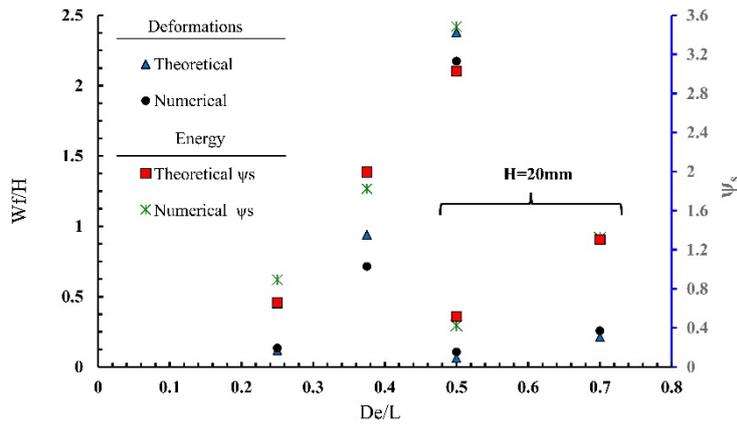
Fig. 27 – The dimensionless energy (ψ_s) predicted theoretically ■ and numerically ✕ on 20mm plate, the dimensionless deformations predicted theoretically ▲ and numerically ● for 10 and 20mm target plate

Fig. 27 also draws a comparison of the normalised energy effectiveness $\psi_s = \frac{1}{2}\mu\dot{w}^2/(HU_c)$, i.e. the ratio of the total initial kinetic energy per area to the total strain energy density through thickness of the material. The kinetic energy reaches its maxima when the load is complete, as time point $t = \tau$ the plate acquires its maximum momentum. Thus, the total transverse velocity of the plate may be quantified as a linear combination of its components through bending and shear sliding mechanisms, using Eq. (57) and $\dot{W} = p_0\tau/\mu$ in Eq. (47). The strain energy density of AR440T (U_c) was evaluated from the quasi static experimental data in Ref. [32]. Since $U_c = \int \sigma_{ij}d\varepsilon_{ij}$ is a scalar parameter-invariant

1   of the loading direction, the total strain energy density of the material is constant and independent of

2   the strain rate or loading conditions.

3   Other forms of the parameter ψ_s exist, such as the energy effectiveness absorbing factor given by

4   [44]. Notwithstanding, to compare the energy effectiveness of various materials, this factor may be

5   generally preferred in contrast to a mere comparison of the materials in terms of the Specific Energy to

6   Tensile Fracture, as it accounts for the plastic work dissipation and shear sliding deformations, given

7   the load parameters of most blast scenarios are known *priori*. A general notion of comparing ductile

8   materials based on their SETF values would lead to inconclusive results as the trend is not

9   straightforward for armour steel plates [45].

10 **5.4   Dynamic pulse loading shape**

11   The analysis in section 4.3 was limited to pulse pressure load having the rectangular shape. A blast

12   peak pressure with dynamic pressure more than 10 times the static collapse can be idealised as

13   rectangular pulse [21]. More often than not, blast loads are non-impulsive which temporal pulse profile

14   may assume various shapes (linear, exponential, sinusoidal). Thus, while the procedure in section 4.3 is

15   maintained, any change in the pulse shape of the load in Eqn. (3) $(p_2(t))$ influences the inertia field

16   across the plate as well as the inertia at the discontinuity front (and their integrals) accordingly. A

17   general expression of the pulse shape introduced by Li and Meng [46] reads:

$$
p_2(t) = \begin{cases} \left(1 - X\dfrac{t}{\tau}\right) e^{-Y\frac{t}{\tau}}, & 0 \le t \le \tau \\[2mm] 0 & \tau \le t \end{cases} \tag{72}
$$

18   While this expression represents a generic exponential function, in particular circumstances it

19   reduces to rectangular pulse (when $X = Y = 0$), or linear pulse (when $X = 1, Y = 0$), as plotted in Fig.

20   28. Taking $X = Y = 1$, for example, the first phase lasts for a duration which yields $T_1 =$

21    $(\tau e^{-1} p_1 \delta)/(12 M_0 b^2 v)$. Thus, the permanent deformation is determined as:

$$
W_f = -\frac{\left(L^2 p_1 T_1^2 \left(\bar{\bar{\xi}} + \frac{1}{2}\right) e^{-\frac{T_1}{\tau}} + 12 M_0 \tau (T_1 + \tau)\right) e^{-\frac{T_1}{\tau}} p_1}{12 M_0 \mu} \tag{73}
$$

22   Occurring at:

$$
T_f = \frac{\left(12 M_0 - L^2 p_1 \bar{\bar{\xi}} e^{-\frac{T_1}{\tau}}\right) T_1}{12 M_0} \tag{74}
$$

23   where $\bar{\bar{\xi}} = \xi_0^3 - \xi_0^2 - \xi_0 - 1$.
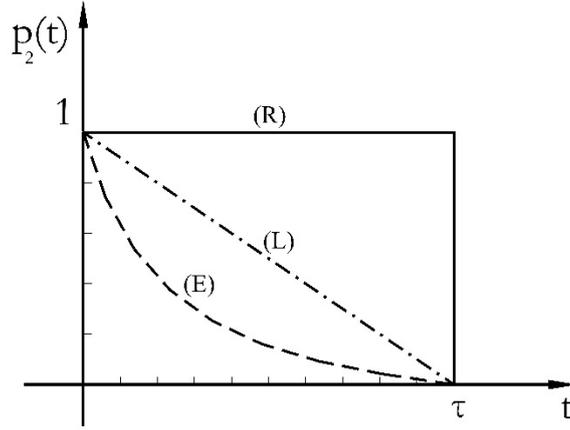
Fig. 28 Typical temporal pulse loading shapes (R) rectngular (L) linear, (E) exponential

1   The permanent deformation of the linearly decaying pulse, with $T_1 = \delta p_1 \tau / (24 M_0 b^2 v)$ can be

2   written as:

$$W_f = -\frac{\left((T_1 - 2\tau)\left((\bar{\bar{\xi}} + 1)\tau^2 + (-2\bar{\bar{\xi}} - 1)T_1\tau + \left(\bar{\bar{\xi}} + \frac{1}{2}\right)T_1^2\right)\eta + 8\beta T_1\tau(T_1 - 3\tau)\right)\eta T_1 p_c}{48\tau^2\beta\mu} \tag{75}$$

3   Occurring at:

$$T_f = \left(\frac{1}{24}\right)\left(L^2(\bar{\bar{\xi}} + 1)\tau^2 - 2T_1 L^2 \bar{\bar{\xi}}\tau + L^2 T_1^2 \bar{\bar{\xi}}\right)\eta/(\tau\beta L^2) + T_1 \tag{76}$$

(a)   (b)
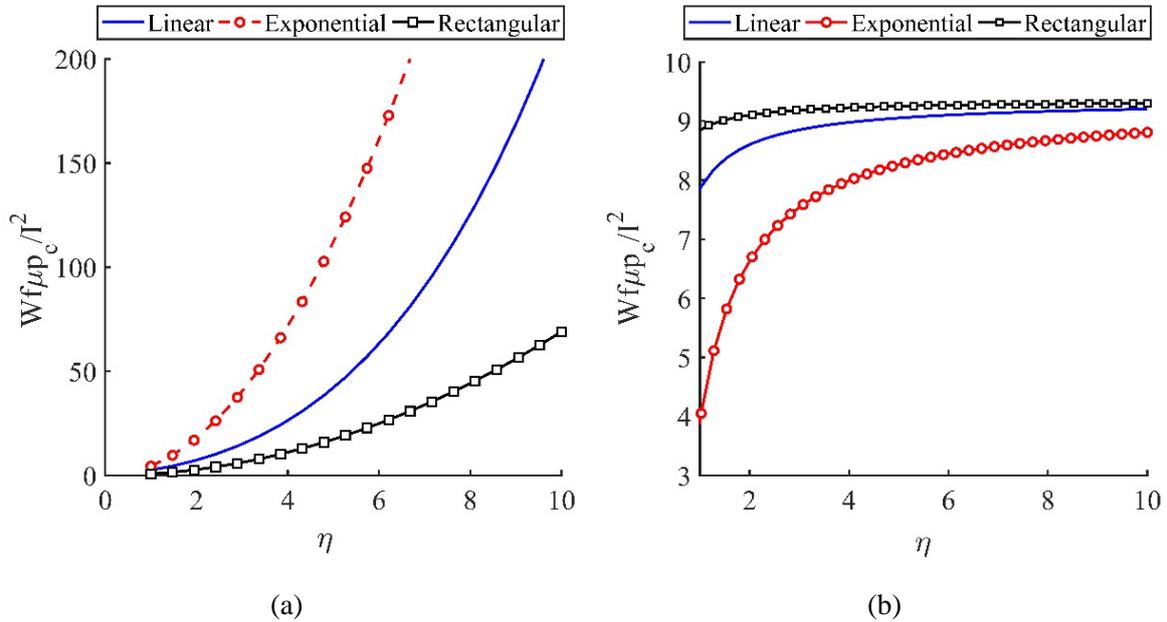
Fig. 29- Pulse shape dependent response with transverse shear effects (a) without transverse shear effects (b) ($b = 50m^{-1}, \omega_0 = 0.05, v = 10$)

4

31
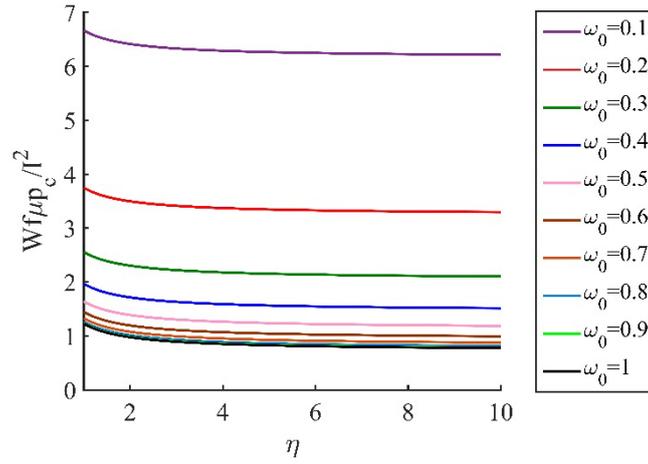
Fig. 30- Pulse shape dependent response of the rectangular pulse with various load radii ($b = 50m^{-1}$, $v = 10$).

1   The pulse shape dependent normalised deformations are plotted in Fig. 29 with and without

2   transverse shear effects, while the influence of the load parameter $\omega_0 = r_e/L$ is graphed in Fig. 30.

3   Clearly, there is a large variation in the normalised deformations due to the pulse shape, which increases

4   with the increase of load magnitude as illustrated in Fig. 29 (a). Obviously, when taking account of the

5   transverse shear effects, the predicted duration of the first phase is influenced by the load magnitude,

6   leading in turn to a divergence of the normalised permanent deformations. In the circumstances where

7   the intrinsic effect of the transverse shear can be neglected and the overall response is pulse dependent

8   (i.e. dynamic or quasi-static), the results of different pressure loads virtually converge to the same value

9   beyond $\eta > 6$ as predicted in Fig. 29 (b). The influence of the load parameter ω_0 on the pulse shape is

10   drawn in Fig. 30.

11   The effect of pulse shapes can be virtually eliminated for monotonically decreasing pressure pulses

12   by incorporating the Youngdahl's correlation parameters in the analysis. There are defined as follows:

$$I_{eff} = \int_{t_0}^{T_f} P(t)dt \tag{77}$$

$$t_m = \frac{1}{I}\int_{t_0}^{T} tP(t)dt \tag{78}$$

$$p_e = \frac{I_{eff}}{2t_m} \tag{79}$$

13   where I_{eff} is the total effective impulse, $P(t) = p_1 p_2(t)$ and p_e is the effective pressure, t_0 is the

14   initial plastic deformation time, taken as zero, assuming the plasticity occurs instantaneously, in other

15   words the chronometer commences operating as plasticity initiates. The time where plastic deformation

16   ceases is denoted as T_f and t_m is the centroid of the pulse. A rectangular pulse, for example, would give

17   rise to $I_{eff} = I = p_1\tau$ and $p_e = p_1$ and centroid of the pulse occurs at $t_m = \tau/2$. Evaluating the above

1   for each pulse shape, a single plot independent of the pulse shape is obtained in terms of the effective

2   pressure and impulse, as given in Fig. 31
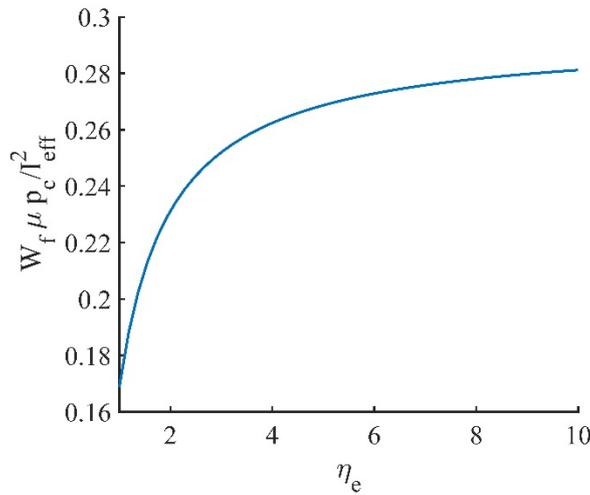
Fig. 31- Pulse shape independent response of the rectangular pulse $(b = 50m^{-1}, \nu = 10, \omega_0 = 0.05)$. $\eta_e = p_e/p_c$ is the effective overloading factor.

3

6   Conclusions

5   In this work, an analytical model was proposed to predict the dynamic plastic response of a generic

6   simply supported, monolithic thick square plate-made of a rate insensitive, ductile metal-subject to

7   dynamic and impulsive localised blasts with the focus on the transverse shear effects. A generic,

8   axisymmetric load was assumed with piecewise continuous function as constant over the central zone

9   with radius r_e, followed by an exponentially decaying spatial variation beyond across the remainder of

10   the target plate. The type of load is universal and adaptable to various blast load scenarios such as those

11   generated from close-in charges to distal charges resulting in a more uniform (global) blasts.

12   While the Mindlin-Reissner plate theory was incorporated in the analyses, the plate was assumed to

13   be sufficiently thick to ignore the build-up of membrane resistance, such that the overall response is

14   governed by the interaction of bending and transverse shear. With idealisation of rigid-perfectly plastic

15   behaviour in mind, the analytical formulations for mid-point and support transverse deformations were

16   obtained in terms of impulsive velocity that incorporates the localisation of the blast. A theoretical

17   analysis on the response of the plate in the range of dynamic blast loads was also presented.

18   The deformations were both affected by the transverse shear in the low range of plate slenderness

19   ratios$(\nu < 2)$. This range of ν is impractical in the design applications of protective systems. The

20   influence of transverse shear on the midpoint and support transverse displacements have been found,

21   which were both affected by the transverse shear in the low range of ν. The influence of transverse shear

22   was found even less significant for the localised blast. The influence of transverse shear sliding was

found infinitesimal for localised blasts, in which case the influence of bending would suffice to estimate the response of the plates.

Parametric studies on impulsively loaded plate showed good correlations between the numerical and analytical models which suggest the adequacy of the analytical model. It must be noted that dynamic pressure and impulse thresholds were kept below the tearing level as ductile fracture related phenomena could not be simulated or presented by rigid-plastic formulation. Finally, a unique pulse shape independent dimensionless response curve was obtained based on Youngdahl's correlation parameters which link model/system and input parameters and are efficient in obtaining results based on effective pressure and impulse loading parameters.

7 Funding

8 Declaration of Conflicting interest

The Authors declare that there is no conflict of interest

9 References

[1]   K. Micallef, A. S. Fallah, D. J. Pope, and L. A. Louca, "Dynamic Performance of Simply Supported Rigid Plastic Circular Thick Steel Plates Subjected to Localized Blast Loading," *J. Eng. Mech.*, no. January, pp. 159–171, 2014.

[2]   G. I. Taylor, "The pressure and Impulse of Submarine Explosion Waves on Plates," *The Scientific Papers of Sir Geoffrey Ingram Taylor*, vol. III, no. 4. Cambridge University Press, Cambridge, UK, pp. 287–303, 1963.

[3]   H. G. Hopkins and W. Prager, "The Load carrying capacity of circular plates," *J. Mech. nd Phys. Solids*, vol. 2, no. June, pp. 1–18, 1953.

[4]   G. S. Langdon, S. C. K. Yuen, and G. N. Nurick, "Experimental and numerical studies on the response of quadrangular stiffened plates. Part II: Localised blast loading," *Int. J. Impact Eng.*, vol. 31, no. 1, pp. 85–111, 2005.

[5]   S. Chung Kim Yuen and G. N. Nurick, "The significance of the thickness of a plate when subjected to localised blast loads," *Blast Impact Load. Struct.*, pp. 471–499, 2000.

[6]   N. K. Gupta and Nagesh, "Deformation and tearing of circular plates with varying support conditions under uniform impulsive loads," *Int. J. Impact Eng.*, vol. 34, no. 1, pp. 42–59, 2007.

[7]   S. B. Menkes and H. J. Opat, "Broken beams - Tearing and shear failures in explosively loaded clamped beams," *Exp. Mech.*, vol. 13, no. 11, pp. 480–486, 1973.

[8]   G. N. Nurick, M. E. Gelman, and N. S. Marshall, "Tearing of blast loaded plates with clamped boundary conditions," *Int. J. Impact Eng.*, vol. 18, no. 7–8, pp. 803–827, 1996.

[9]   N. Jacob, G. N. Nurick, and G. S. Langdon, "The effect of stand-off distance on the failure of fully clamped circular mild steel plates subjected to blast loads," *Eng. Struct.*, vol. 29, no. 10, pp. 2723–2736, 2007.

[10] Q. M. Li, "Continuity conditions at bending and shearing interfaces of rigid, perfectly plastic structural elements," *Int. J. Solids Struct.*, vol. 37, no. 27, pp. 3651–3665, 2000.

[11] Q. M. Li and N. Jones, "On dimensionless numbers for dynamic plastic response of structural members," *Arch. Appl. Mech.*, vol. 70, no. February 1999, pp. 245–254, 2000.

[12] N. Jones and N. Jones, "Bounds On The Dynamic Plastic Behaviour of Structures IncludingTransverse Shear Effects," *Int. J. Impact Eng.*, vol. 3, no. 4, pp. 273–291, 1985.

[13] N. Jones and J. Gomes De Oliveira, "Dynamic Plastic Response of Circular Plates With Transverse Shear and Rotatory Inertia," *J. Appl. Mech.*, vol. 47, no. March 1980, pp. 27–34, 1980.

[14] N. Jones and J. Gomes De Oliveira, "The Influence of Rotatory Inertia and Transverse Shear on the Dynamic Plastic Behavior of Beams," *J. Appl. Mech.*, vol. 46, no. June 1979, pp. 303–310, 1979.

[15] J. Gomes de Oliveira and N. Jones, "A Numerical Procedure for the Dynamic Plastic Response of Beams with Rotatory Inertia and Transverse Shear Effects," *J. Struct. Mech.*, vol. 7, no. 2, pp. 193–230, 1979.

[16] Q. M. Li and N. Jones, "Blast loading of fully clamped circular plates with transverse shear effects," *Int. J. Solids Struct.*, vol. 31, no. 14, pp. 1861–1876, 1994.

[17] Q. M. Li and N. Jones, "Blast Loading of Fully Clamped Beams with Transverse Shear Effects," *Mech. Struct. Mach.*, vol. 23, no. 1, pp. 59–86, 1995.

[18] Q. M. Li and N. Jones, "Blast loading of a 'short' cylindrical shell with transverse shear effects," *Int. J. Impact Eng.*, vol. 16, no. 2, pp. 331–353, 1995.

[19] R. Zaera, A. Arias, and C. Navarro, "Analytical modelling of metallic circular plates subjected to impulsive loads," *Int. J. Solids Struct.*, vol. 39, no. 3, pp. 659–672, 2002.

[20] Q. M. Li and Y. G. Huang, "Dynamic plastic response of thin circular plates with transverse shear and rotatory inertia subjected to rectangular pulse loading," *Int. J. Impact Eng.*, vol. 8, no. 3, pp. 219–228, 1989.

[21] N. Jones, *Structural Impact*, 1st ed. Cambridge: Cambridge University Press, 1997.

[22] W. J. Stronge and T. X. Yu, *Dynamic Models for Structural Plasticity*. London: Springer, 1993.

[23] D. Karagiozova, G. S. Langdon, G. N. Nurick, and S. Chung Kim Yuen, "Simulation of the response of fibre-metal laminates to localised blast loading," *Int. J. Impact Eng.*, vol. 37, no. 6, pp. 766–782, 2010.

[24] C. K. Youngdahl, "Correlation parameters for eliminating the effects of pulse shape on dynamic plate deformation," *Trans. ASME J. Appl. Mech.*, vol. 37, no. 2, pp. 744–752, 1970.

[25] C. K. Youngdahl, "Influence of pulse shape on the final plastic deformation of a circular plate," *Int. J. Solids Struct.*, vol. 7, no. 9, pp. 1127–1142, 1971.

[26] K. Micallef, a. S. Fallah, D. J. Pope, and L. A. Louca, "The dynamic performance of simply-supported rigid-plastic circular steel plates subjected to localised blast loading," *Int. J. Mech. Sci.*, vol. 65, no. 1, pp. 177–191, 2012.

[27] Q. M. Li and N. Jones, "Foundation of Correlation Parameters for Eliminating Pulse Shape Effects on Dynamic Plastic Response of Structures," *J. Appl. Mech.*, vol. 72, no. 2, p. 172, 2005.

[28] Y. Yuan, P. J. Tan, K. A. Shojaei, and P. Wrobel, "Large deformation, damage evolution and failure of ductile structures to pulse-pressure loading," *Int. J. Solids Struct.*, vol. 96, pp. 320–339, 2016.

[29] S. E. Rigby *et al.*, "Measuring spatial pressure distribution from explosives buried in dry

Leighton Buzzard sand," *Int. J. Impact Eng.*, vol. 96, pp. 89–104, 2016.

[30] A. D. Cox and L. W. Morland, "Dynamic plastic deformations of simply-supported square plates," *J. Mech. Phys. Solids*, vol. 7, no. March 1959, pp. 229–241, 1959.

[31] S. Timoshenko, S.;Woinosky-Kreiger, *Theory of Plates and Shells*. New York: McGraw Hill, 1959.

[32] N. Mehreganian, L. A. Louca, G. S. Langdon, R. J. Curry, and N. Abdul-Karim, "The response of mild steel and armour steel plates to localised air-blast loading-comparison of numerical modelling techniques," *Int. J. Impact Eng.*, vol. 115, no. May, pp. 81–93, 2018.

[33] T. Børvik, A. G. Hanssen, M. Langseth, and L. Olovsson, "Response of structures to planar blast loads - A finite element engineering approach," *Comput. Struct.*, vol. 87, no. 9–10, pp. 507–520, 2009.

[34] W. Grobbelaar and G. Nurick, "An investigation of Structures Subjected to Blast Loads Incorporating an Equation of State to Model the Material Behaviour of the Explosives," in *7th International Symposium on Structural Failure and Plasticity (IMPLAST 2000)*, 2000, pp. 185–194.

[35] B. Zakrisson, B. Wikman, and H. K. Häggblad, "Numerical simulations of blast loads and structural deformation from near-field explosions in air," *Int. J. Impact Eng.*, vol. 38, no. 7, pp. 597–612, 2011.

[36] SSAB, "Armox Blast Protection Plate," *SSAB Swedish Steel Ltd*, 2018. [Online]. Available: https://www.ssab.co.uk/products/brands/armox. [Accessed: 04-Jun-2018].

[37] B. McDonald, H. Bornstein, A. Ameri, J. P. Escobedo-Diaz, and A. Orifici, "High strain rate and high temperature response of two armour steels: Experimental testing and constitutive modelling," in *Proceedings of the 12th International DYMAT Conference*, 2018, vol. 01022, pp. 1–6.

[38] Dassault Systèmes Simulia, "Abaqus 6.1 2 (Analysis User's Manual)," vol. V. 2012.

[39] D. Bonorchis and G. N. Nurick, "The influence of boundary conditions on the loading of rectangular plates subjected to localised blast loading - Importance in numerical simulations," *Int. J. Impact Eng.*, vol. 36, no. 1, pp. 40–52, 2009.

[40] K. Micallef, A. Soleiman Fallah, D. J. Pope, M. Moatamedi, and L. A. Louca, "On dimensionless loading parameters for close-in blasts," *Int. Jounral Multiphysics*, vol. 9, no. 2, pp. 171–194, 2015.

[41] N. Mehreganian, A. S. Fallah, G. K. Boiger, and L. A. Louca, "Reponse of armour steel square plates to localised air blast loading- A dimensional analysis," *Int. J. Multiphys.*, vol. 11, no. 4, pp. 387–412, 2017.

[42] N. . Mehreganian, A. S. . Fallah, and L. A. . Louca, "Inelastic dynamic response of square membranes subjected to localised blast loading," *Int. J. Mech. Sci.*, vol. 148, no. September, pp. 578–595, 2018.

[43] D. Bonorchis and G. N. Nurick, "The effect of welded boundaries on the response of rectangular hot-rolled mild steel plates subjected to localised blast loading," *Int. J. Impact Eng.*, vol. 34, no. 11, pp. 1729–1738, 2007.

[44] N. Jones, "Energy-absorbing effectiveness factor," *Int. J. Impact Eng.*, vol. 37, no. 6, pp. 754–765, 2010.

[45] B. McDonald, H. Bornstein, G. S. Langdon, R. Curry, A. Daliri, and A. C. Orifici, "Experimental response of high strength steels to localised blast loading," *Int. J. Impact Eng.*, vol. 115, no. October 2017, pp. 106–119, 2018.

[46] Q. M. Li and H. Meng, "Pulse loading shape effects on pressure-impulse diagram of an elastic-plastic, single-degree-of-freedom structural model," *Int. J. Mech. Sci.*, vol. 44, no. 9, pp. 1985–

1   1998, 2002.
2